Bulletin of the New Zealand Society for Earthquake Engineering, Vol. 50, No. 1, March 2017

THE NEW ZEALAND STRONG MOTION DATABASE

Chris Van Houtte[1,2], Stephen Bannister[3], Caroline Holden[4], Sandra Bourguignon[5] and Graeme McVerry[6]

(Submitted *May 2016*; Reviewed *August 2016;* Accepted *November 2016*)

ABSTRACT

This article summarises work that has been undertaken to compile the New Zealand Strong Motion Database, which is intended to be a significant resource for both researchers and practitioners. The database contains 276 New Zealand earthquakes that were recorded by strong motion instruments from GeoNet and earlier network operators. The events have moment magnitudes ranging from 3.5 to 7.8. A total of 134 of these events (49%) have been classified as occurring in the overlying crust, with 33 events (12%) located on the Fiordland subduction interface and 7 on the Hikurangi subduction interface (3%). 8 events (3%) are deemed to have occurred within the subducting Australian Plate at the Fiordland subduction zone, and 94 events (34%) within the subducting Pacific Plate on the Hikurangi subduction zone. There are a total of 4,148 uniformly-processed recordings associated with these earthquakes, from which acceleration, velocity and displacement time-series, Fourier amplitude spectra of acceleration, and acceleration response spectra have been computed. 598 recordings from the New Zealand database are identified as being suitable for future use in time-domain analyses of structural response. All data are publicly available at http://info.geonet.org.nz/x/TQAdAQ.

INTRODUCTION

The main objective of the New Zealand Strong Motion Database is to provide users of strong motion data, both in the research and consulting communities, with consistently determined data of the highest possible quality. This article details the methods used to calculate the source and path parameters for large New Zealand earthquakes that occurred between 1968 and 2016, as well as detailing the record processing and associated ground motion intensity variables. The methods adopted to calculate quantitative subsurface information at GeoNet strong motion sites are discussed in the companion article of Kaiser et al. (2016) [1]. The intent of this article is to provide potential users of the database with comprehensive documentation, such that it is possible to independently evaluate the suitability of the database for a given analysis. While there have previously been large, nationwide collations of strong motion data in New Zealand for the purposes of ground motion modelling ([2-4]), this database is the first in New Zealand that is publicly available and fully documented.

The primary source parameters provided in the database are the seismic moment magnitude (M_w), preferred location, origin time, focal mechanism, and tectonic classification (e.g. crustal, subduction interface or subducted slab). Where available, published models of an earthquake's co-seismic slip distributions have been prepared and supplied in a common electronic format.

Additional information on the seismic wave propagation path is also provided, including focal depths, hypocentral distances and epicentral distances. Distances to the rupture surface, such as the depth to the top of the rupture (Z_{TOR}), the closest Cartesian distance between the recording site and the rupture (R_{rup}), and the Joyner-Boore distance (R_{JB}) have also been defined. These distances are measured with respect to a fault geometry model, where available. For smaller magnitude events, these quantities are calculated with respect to an inferred fault plane.

All of the 4,148 seismic records in the database have been visually examined for quality and manually processed. The main objective of the strong-motion processing is to allow the data to be used for subsequent engineering analysis, by correcting for the response of the instrument and reducing the effect of noise in the signal. From the processed time-series, Fourier amplitude spectra of acceleration and acceleration response spectra have been pre-calculated. The resultant database is openly available at info.geonet.org.nz/x/TQAdAQ. Note that the processed accelerograms are different from those found at GeoNet's collection of strong motion data (ftp.geonet.org.nz/strong/processed/Proc), due to the reprocessing of data in this study.

It is intended to periodically update the source and waveform databases when new earthquake data becomes available. Additionally, the data associated with older events may be reanalysed as seismological analysis techniques are improved.

SOURCE INFORMATION

Selection of Events

The selection of events to include in the database required some decisions on data quality. Strong motion database development is a trade-off between quality and quantity. Including low quality data increases the sample size, but has the shortcoming that inferences from the data are not necessarily robust. In this study, it was preferred to apply a minimum standard for data quality. For example, one key criterion was that for an event to be considered, it must have an M_w that is derived from the seismic moment, rather than inferred from correlations with other magnitude measures. In general, events were also required to have a minimum of three usable recordings, but this criterion was occasionally relaxed

[1] *Corresponding Author, Engineering Seismologist, GNS Science, Lower Hutt, c.vanhoutte@gns.cri.nz (Member)*
[2] *Fellow, Harvard University, Massachusetts, United States*
[3] *Principal Scientist and Team Leader Seismology, GNS Science, Lower Hutt*
[4] *Seismologist, GNS Science, Lower Hutt (Member)*
[5] *Seismologist, GNS Science, Lower Hutt*
[6] *Principal Scientist and Engineering Seismologist, GNS Science, Lower Hutt (Life Member)*

for older events in the database. Older events tend to be poorly recorded and located, but they were included in the database if they were considered to be potentially informative datasets.

Given these criteria, this database is not intended to be a complete representation of all large events to have occurred in New Zealand, and is only a selection of well-recorded events that are suitable for modelling of ground motion. However, it was endeavoured to include the majority of earthquakes with M_w greater than 5.

Calculation of Magnitudes and Associated Uncertainty

Earthquake magnitudes are useful for quantifying the rupture size or the energy released by an earthquake. There are many different types of earthquake magnitude. For most engineering purposes, the magnitude of interest is the moment magnitude, M_w, which is related to the total rupture area and the amount of slip that occurred in the earthquake. M_w is typically calculated from the seismic moment, M_0, using the equation from Kanamori (1977) [5]

$$M_w = \frac{2}{3}\log_{10}(M_0) - 6.03 \quad (1)$$

where M_0 has units of Nm. M_0 can be calculated using a number of different inversion approaches and datasets, and can have variability even for the same earthquake. Kagan (2002) [6] investigated the difference in M_w values calculated from nine different catalogues in California, and found systematic differences between some catalogues, and in some cases, significant scatter. The uncertainty in M_0, and therefore M_w, can affect subsequent analyses of the dataset, hence some effort has been made to quantify this uncertainty for New Zealand earthquakes.

A systematically-calculated national catalogue of M_0 for New Zealand earthquakes is not available for events before 2003. For events before 2003, M_0 values were calculated either by special studies, or from a global database. The M_0 values in the database are therefore collated from a number of different sources. For example, 17 events in the database between 1968 and 1993 have M_0 values calculated in special studies using waveform modelling of teleseismic data (e.g. [7, 8]). The introduction of the Global Centroid Moment Tensor (CMT) catalogue in 1976 (formerly known as Harvard CMT solutions; [9]) provided an additional source of M_0 values for many large events, again calculated using teleseismic data. Estimating moment tensor solutions from regional data was not feasible before 2003, due to the sparse seismograph network [10]. Since the introduction of GeoNet (www.geonet.org.nz), the denser seismograph network in New Zealand has enabled the calculation of regional moment tensor (RMT) solutions, and subsequently GeoNet have provided a large catalogue of RMT solutions [11, 12] from 2003 onwards.

In some cases, more than one M_0 value is available for the same event. Previous studies have examined the differences between methods of calculating M_0 (and therefore M_w) in New Zealand. Dowrick and Rhoades (1998) [13] compared locally-determined M_w values with Global CMT values, finding no systematic differences but a standard deviation of 0.08 magnitude units. Ristau (2009) [14] found no significant difference between M_w calculated using RMTs and Global CMTs for 25 events that occurred between 2003 and 2008, however this comparison is revisited in this study, given the many large earthquakes in New Zealand between 2009 and 2015. Figure 1 shows the difference between the two catalogues for 52 events. There are two features from this plot that warrant discussion. Firstly, the Global CMT M_w values are clearly larger than GeoNet RMT M_ws where the GeoNet M_w is less than 5.0. It is unclear what causes this discrepancy, given that the two solutions analyse different frequency bands, although it is likely that the GeoNet RMT is derived from a stronger signal. Secondly, the scatter in the calculated M_w values from the different catalogues appears to increase with magnitude. This observation contrasts with the M_w uncertainties assigned in the NGA-West2 database [15], which tend to give smaller 'statistical uncertainty' in M_w (i.e. standard deviation of good-quality published values) with increasing magnitude. However, given that there are few data at large magnitudes, a magnitude-independent standard deviation of 0.06 magnitude units (determined from the residuals of the linear model in Figure 1, for magnitudes greater than 5.0) has been adopted for simplicity.

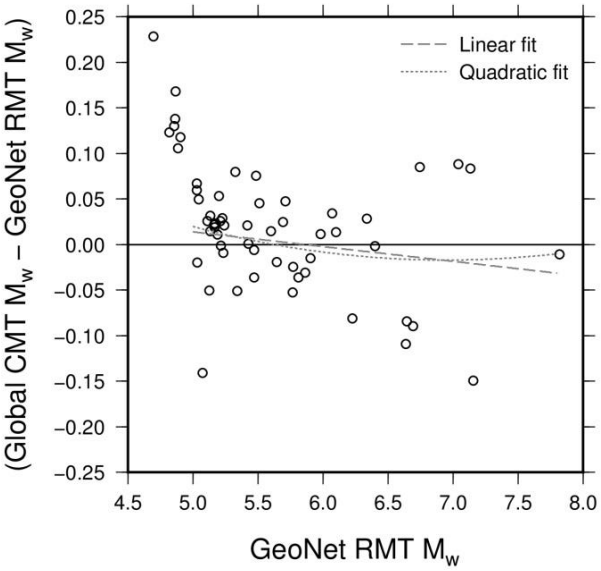

Figure 1: Comparison of GeoNet RMT M_w and Global CMT M_w for all New Zealand earthquakes since 2003, where a value is available from both catalogues.

None of the catalogues publish uncertainties with their own calculated M_w values, as this is difficult to calculate using current methods. However, to acknowledge the uncertainty in M_w, the following decisions have been made for the New Zealand Strong Motion Database:

- to assign M_w values for each event:
  - where more than one M_w value is available, the average value is taken; and,
  - for magnitudes less than 5.0, M_w is taken from the GeoNet RMT catalogue, as this is deemed to be the most reliable solution.
- to assign a standard deviation value:
  - events before 2003, where only a single locally-determined M_w or Global CMT solution is available, are assigned a standard deviation of 0.15;
  - events after 2003, where only a single RMT or Global CMT is available, are assigned a standard deviation of 0.1;
  - for events where both a locally-determined M_w from special studies and a Global CMT M_w are available, the standard deviation is 0.08 magnitude units (the value given in [13]); and,
  - if events have both a regional and global moment tensor solution available, the standard deviation is 0.06.

These standard deviation values are of a similar order to those defined in Rhoades (1997) [16]. Propagating the magnitude uncertainty into empirical ground-motion models influences the model parameters and the overall model uncertainty, and can have a large influence on seismic hazard estimates at low probabilities of exceedance [3, 16, 17]. The online files for the New Zealand database contain references showing where the

M_w values were obtained. Figure 2 shows a histogram of moment magnitudes for all the events in the database.

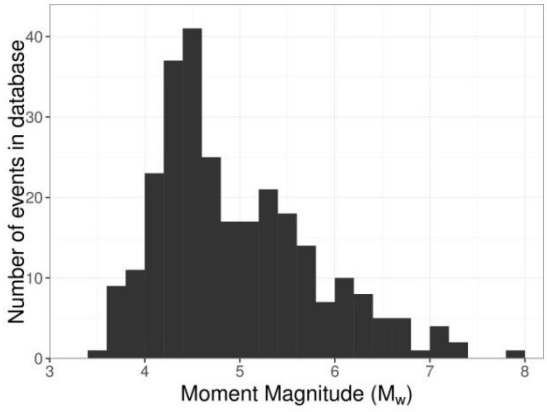

Figure 2: Magnitudes in the database.

Focal Mechanisms

Each event in the database has a published moment tensor solution. The moment tensor solutions are obtained from the GCMT catalogue and the GeoNet RMT catalogue. In general, these catalogues agree well with each other. In the case of multiple solutions, the preferred solution (generally the GeoNet RMT solution) has been indicated in the database source table. For the 276 events in the catalogue, 79 of the events have strike-slip mechanisms, 65 are reverse, 27 are oblique, 48 are normal, while for 57 events, the mechanism could not be determined from the moment tensor. This is illustrated in Figure 3. However, while the mechanism can be determined for almost 80% of the events, a preferred orientation of the actual fault plane has been indicated for only 87 of the 276 events, 32% of the events. For these events, the rake angle is provided.

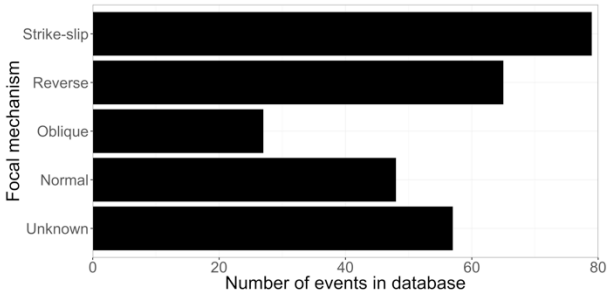

Figure 3: Summary of focal mechanisms in the database.

Event Locations

Research has shown that using high-quality earthquake source locations improves subsequently-developed ground motion models, particularly for short-period response spectra [18]. As such, effort was made to obtain the best quality locations. Earthquake locations in New Zealand tend to be poorly constrained, particularly for older events in the database. The hypocentral locations for the 276 events in the database have been determined using a number of methods. In most cases, more than one solution is available for each event. There are three existing catalogues from which earthquake locations are determined: special studies, the standard GeoNet catalogue [19], a relocated New Zealand catalogue between 2001 and 2012 [20], and the International Seismological Centre (ISC) catalogue [21]. Additionally, all events in the database were relocated as part of this study, using a probabilistic, nonlinear source location algorithm called NonLinLoc [22, 23].

The special studies catalogue mainly applies to the older events in the database e.g. [7, 8]. These studies used P and SH body-wave modelling to derive focal mechanisms, then the depth was fixed at the minimum misfit solution before relocating the event using regional and teleseismic data. The locations provided in the standard GeoNet catalogue were determined by GeoNet (and earlier by DSIR) using a variety of approaches. For events before 1987, the locations were determined using software known as LOCAL [24], in conjunction with three 1D velocity models for different locations around New Zealand. Between 1987 and 2012, events were located using the GROPE technique within the Caltech-USGS Seismic Processing (CUSP) system, using updated 1D velocity models. Since 2012, GeoNet now use two techniques to locate events, the LocSAT program [25] in conjunction with the IASPEI91 1D reference earth model [26], and the NonLinLoc algorithm in conjunction with the New Zealand 3D velocity model [27]. Only local and regional data are used by GeoNet to derive the locations in their catalogue. Full details on GeoNet locations can be found on the GeoNet website [28]. A separate catalogue of relocated seismicity, by Reyners *et al*. (2011) [20], uses the simulPS algorithm [29, 30] within the New Zealand 3D velocity model. The final catalogue used for the database, the ISC catalogue, uses regional and global data to locate events using the ak135 velocity model [31], and a linearised inversion algorithm [32]. To supplement these catalogues, and improve location estimates for older events in the New Zealand Strong Motion Database, all events in the database were relocated using local data and the New Zealand 3D velocity model, applying the NonLinLoc algorithm.

The preferred location (in the opinion of the authors) was then selected from all of the alternative solutions. While it is difficult to ascertain the most likely location of an event, the locations from the special studies were preferred over other methods, typically followed by a preference for the 3D relocations derived using the simulPS algorithm. In general, locations of nearly all offshore earthquakes are poorly constrained, as are locations for events occurring before the development of the GeoNet seismometer network in 2001.

Tectonic Classification

Crustal, subduction interface and intra-slab earthquakes are usually treated separately in ground-motion prediction models. These categories of earthquakes may have different source characteristics, and the seismic waves may have very different travel paths. The separation of events into these categories is largely based on expert judgement. In general, when the event is located away from the Hikurangi and Fiordland subduction interfaces, it was simple to classify these events as being in the seismogenic zone of the crust. The boundary between the upper crust and the mantle can be approximately defined as the depth where the P-wave velocity is equal to ~8.5 km/s. The only crustal events in the database that approach this depth are in the Manuwatu-Whanganui region, and most crustal events are significantly shallower than this boundary.

Near the interfaces of the Hikurangi and Fiordland subduction zones, it is more difficult to classify events as being in the overlying crust, on the subduction interface or in the subducting crust. However, a number of tools were utilised to help with correctly classifying these events. For events around the Hikurangi subduction interface, all event location solutions were compared to the Hikurangi subduction interface model of

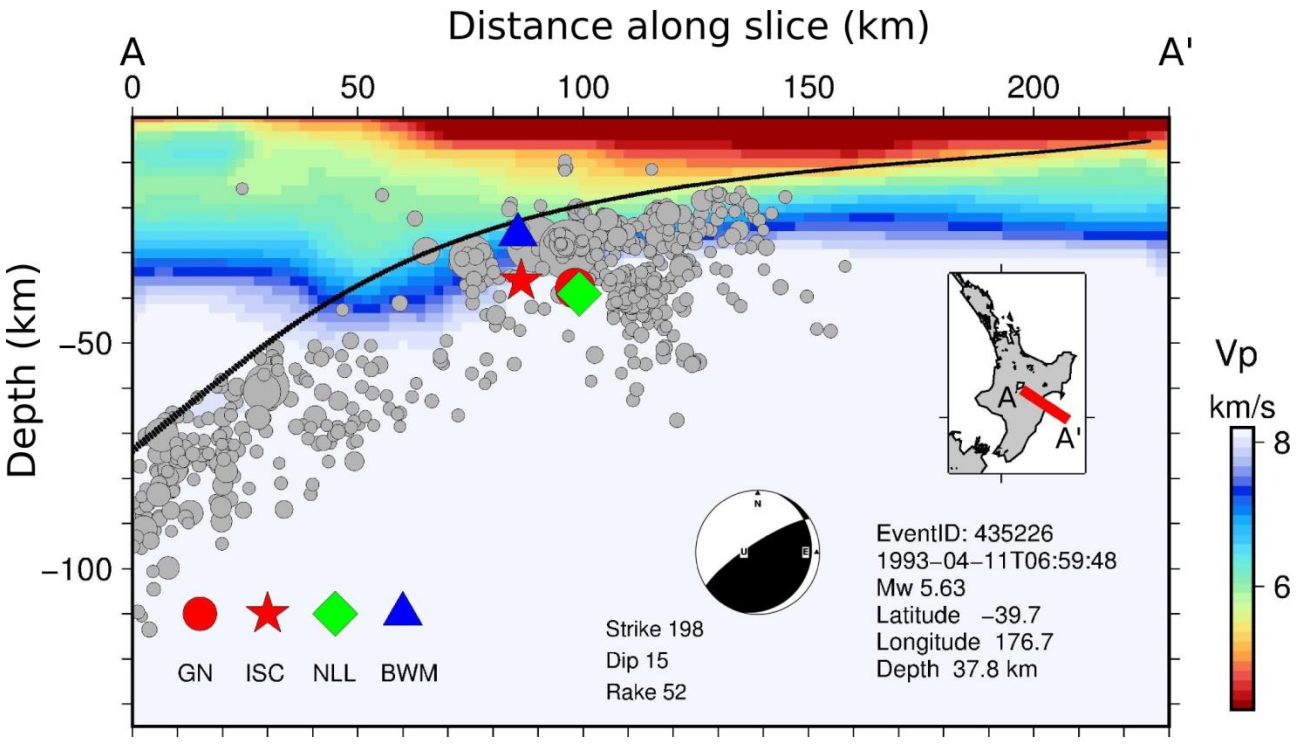

Figure 4: Plots used to determine preferred earthquake location and subsequent tectonic classification in the North Island, with the 1993 Tikokino earthquake as an example. This is a slice of the New Zealand velocity model [27], with the Williams et al. (2013) [33] Hikurangi subduction interface model indicated as a black line, and relocated seismicity between 2001 and 2012 [20] as grey circles. Different hypocentre solutions are: GN = GeoNet catalogue, ISC = International Seismological Centre catalogue, NLL = NonLinLoc solution and BWM = body wave modelling. The focal mechanism (plotted as an upper hemisphere) is a shallow-angle oblique thrust with similar strike to the Hikurangi margin. In this instance, the BWM solution [8] was selected as the preferred location, and the event was considered likely to have occurred on the subduction interface.

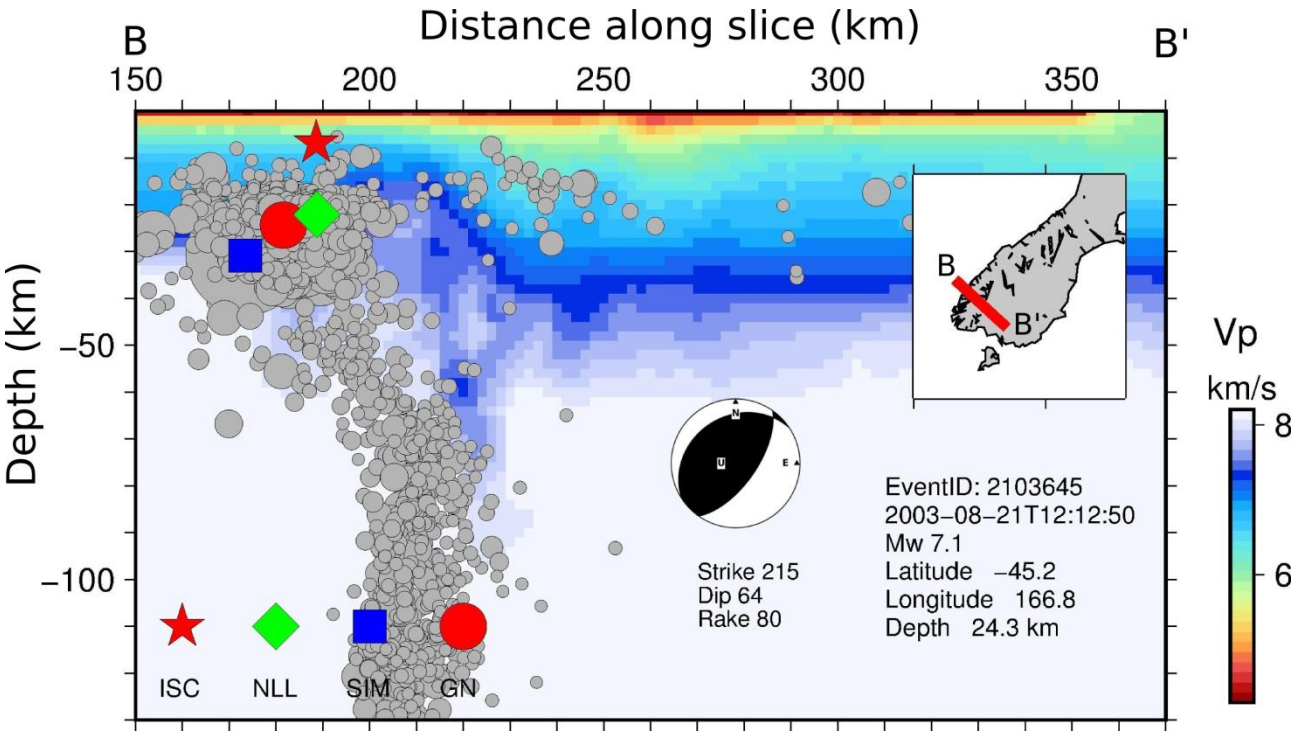

Figure 5: Example of plot used to determine earthquake location in Fiordland, for which no interface model is available, using the example of the 2003 M_w7.2 Fiordland earthquake. This plot is similar to Figure 4, but SIM = the simulPS solution. In this instance, the NonLinLoc solution is preferred and the event was classified as occurring on the subduction interface, consistent with the focal mechanism.

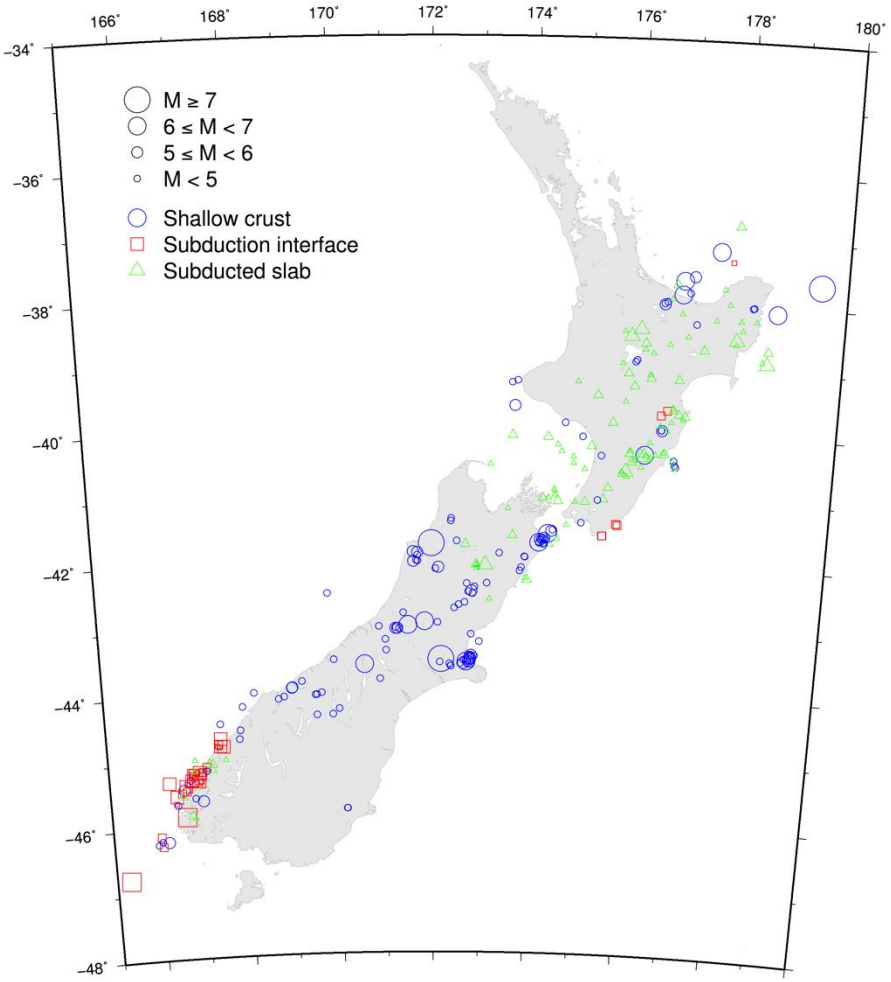

Figure 6: Event locations and tectonic classifications, for all events in the database.

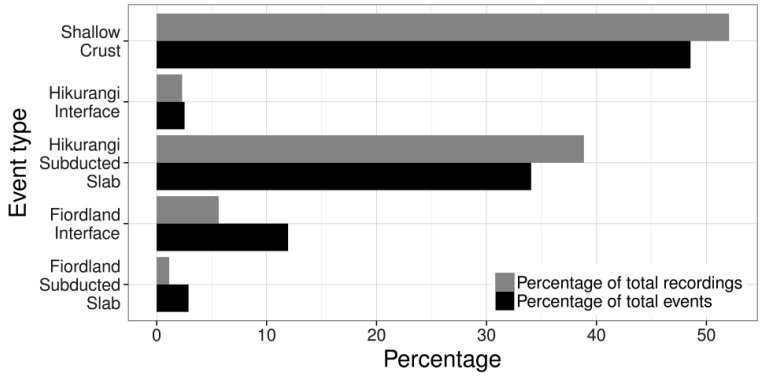

Figure 7: Tectonic classifications as a proportion of the total dataset.

Williams *et al*. (2013) [33], along with all of the relocated seismicity from 2001-2012 [20]. These locations were examined together with the focal mechanism, and judgement was then used to decide on a preferred event classification. Refer to the example shown in Figure 4. In this case, it is rather unclear from the event locations whether this particular event is on the interface, just above in the overlying crust, or in the subducted crust. However, the mechanism shows a shallow-angle thrusting event with similar strike and dip to the Williams *et al*. (2013) model, which suggests that this event is likely to have occurred on the subduction interface.

The geometry of the Fiordland subduction interface is very uncertain, with only schematic interpretations available from Eberhart-Phillips & Reyners (2001) [34] and Reyners *et al*. (2002) [35]. In general, the event locations are also less reliable in Fiordland, due to the sparse seismometer network in that region, so more emphasis is placed on the focal mechanism to determine the tectonic classification. An example of the M_w7.3 Fiordland event in 2003 is shown in Figure 5. Although the event locations are rather scattered, the strike and dip of reverse/oblique mechanism indicates that this event was likely to have occurred on the plate interface.

In many cases, the evidence for the tectonic classification was not compelling. While the assigned classifications are uncertain and should be considered indicative only, the classifications have been selected based on the best available information to the authors at the time of writing. The tectonic classifications in terms of hypocentral locations are shown on the map in Figure 6, while Figure 7 shows the percentage of total events and total recordings corresponding to each classification.

Table 1: Events with published slip distributions, and events with published preferred fault plane orientations.

Year	Name	Mw	Strike (deg)	Dip (deg)	Rake (deg)	Fault length (km)	Fault width (km)	Z_{TOR} (km)	Latitude (top centre)	Longitude (top centre)	Method	Reference for preferred model	References for alternative models
1968	Inangahua	7.23	207	45	103	30	10.5	0	-41.91	171.95	1	Anderson et al. (1994) [36]	
1985	Tiniroto	5.97	213	73	255	11	11	26	-38.73	177.32	3	Reyners et al. (2010) [37]	
1987	Edgecumbe*	6.49	225	45	-110	-	-	0	-	-	1	Beanland et al. (1990) [38]	
1988	Te Anau	6.69	310	86	118	25	55	35	-45.11	167.15	3	Robinson et al. (2003) [39]	Reyners et al. (1991) [40]
1989	Doubtful Sound	6.39	139	67	47	15	15	14	-45.24	166.94	3	Robinson et al. (2003) [39]	
1990	Lake Tennyson	5.96	55	89	163	8	5	6	-42.25	172.74	3	McGinty & Robinson (1999) [41]	
1990	Weber 1	6.24	209	72	-112	13	13	18	-40.39	176.24	3	Robinson (1994) [42]	Reyners et al. (2010) [37]
1990	Weber 2	6.39	220	28	149	12.5	12.5	9	-40.38	176.28	3	Robinson (1994) [42]	
1990	Cape Palliser 1	5.57	190	21	58	4.5	4.5	13	-41.61	175.45	3	Luo (1992) [43]	
1990	Cape Palliser 2	5.46	250	38	145	4	4	13	-41.62	175.43	3	Luo (1992) [43]	
1993	Secretary Island	6.89	41	41	107	26	14.5	11.5	-45.15	166.69	3	Robinson et al. (2003) [39]	
1993	Ormond	6.30	354	64	168	30	15	32	-38.55	177.88	3	Reyners et al. (2010) [37]	
1994	Arthur's Pass	6.72	221	47	112	16	12	1	-43.04	171.51	3	Abercrombie et al. (2000) [44]	Robinson et al. (1995) [45]
1995	Cass	6.19	176	46	44	12	6	1	-42.94	171.86	3	Gledhill et al. (2000) [46]	
2000	Thompson Sound	6.13	171	57	59	12.5	12.5	14	-45.12	167.04	3	Robinson et al. (2003) [39]	
2003	Fiordland	7.17	35	23	95	60	50	10	-45.11	166.87	3	McGinty & Robinson (2007) [47]	Reyners et al. (2003) [48]
2005	Upper Hutt	5.31	70	48	-75	4	3	30	-41.09	175.06	3	Reyners et al. (2010) [37]	
2007	George Sound	6.79	54	44	129	25	12	16	-44.78	167.33	2	Petersen et al. (2009) [49]	
2007	Gisborne	6.65	71	45	300	12	14	43	-38.87	178.49	2	François-Holden et al. (2008) [50]	Reyners et al. (2010) [37]
2008	Hastings	5.43	1	38	-113	5	5	28	-39.65	176.73	3	Reyners et al. (2010) [37]	
2009	Dusky	7.81	27	33	154	36	44	9	-45.74	166.09	2	Fry et al. (2010) [51]	Beavan et al. (2010) [52]
2010	Darfield*	7.08	-	-	-	-	-	0	-	-	1	Beavan et al. (2012) [53]	Holden et al. (2011) [54], Barnhart et al. (2011) [55], Elliot et al. (2012) [56], Atzori et al. (2012) [57]
2011	Christchurch February	6.19	59	67	136	8	10	0.5	-43.53	172.72	2	Holden (2011) [58]	Barnhart et al. (2011) [55], Beavan et al. (2012) [53], Elliot et al. (2012) [56], Atzori et al. (2012) [57], Serra et al. (2013) [59]
2011	Christchurch June*	5.99	-	-	-	-	-	3	-	-	2	Holden & Beavan (2012) [60]	Beavan et al. (2012) [53], Elliot et al. (2012) [56], Atzori et al. (2012) [57]
2011	Pegasus 1	5.79	45	63	105	3	10	1	-43.47	172.78	2	Ristau et al. (2013) [61]	
2011	Pegasus 2	5.85	57	51	123	6	10	1	-43.47	172.76	2	Ristau et al. (2013) [61]	Beavan et al. (2012) [53]
2013	Cook Strait	6.58	234	75	164	13	12	7	-41.63	174.31	2	Holden et al. (2013) [62]	Hamling et al. (2014) [63]
2013	Lake Grassmere	6.60	234	74	168	18	18	1.5	-41.72	174.18	1	Hamling et al. (2014) [63]	Holden et al. (2013) [62], Kaneko et al. (2016) [64]
2014	Eketahuna	6.31	213	56	247	8	10	32	-40.61	175.83	2	Holden (unpublished)	
2016	Christchurch Valentines	5.76	58	72	156	5	9	4	-43.47	172.78	2	Kaiser et al. (2016) [64] seismic	Kaiser et al. (2016) [64] geodetic

For 'method',

1 = Slip distribution obtained by inversion of geodetic data. Fault size and co-ordinates are only indicative, as source-to-site distances are measured to the closest point on the fault where the slip is greater than or equal to 50 cm.

2 = Co-seismic slip distribution obtained by inversion of seismic data.

3 = Extent of fault plane approximated from aftershock distributions.

* Fault geometry parameters not provided due to complex rupture. See web repository for fault model, if available.

MODELS OF RUPTURE SURFACES

Published Source Models

For large earthquakes, defining the rupture surface is important for deriving source-to-site distance metrics. While moment tensor solutions define the focal mechanism with two possible orthogonal fault planes, the orientation and size of the true rupture area needs to be determined using other methods. The fault geometry and orientation can be obtained from observed surface rupture, by inverting for the co-seismic slip distribution using either seismic or geodetic data, or by observing aftershock distributions.

Three earthquakes in the database have observed, onshore, surface ruptures: the 1968 Inangahua earthquake, 1987 Edgecumbe earthquake and the 2010 Darfield earthquake. Both the Edgecumbe and Darfield events had complex geometries, with the Edgecumbe earthquake having eleven observed segments rupturing the ground surface [38], and the Darfield earthquake having three distinct right-lateral segments in the surface rupture [65]. In the Inangahua event, surface rupture was observed in numerous locations, and the event had a complex source-time function, which also suggests multi-segment rupture [36].

Twelve earthquakes have co-seismic slip distributions, determined either by inverting seismic waveform or geodetic data, or both. For the cases where more than one model of the slip distribution was available, the merits of alternative models were examined in detail before the selection of a preferred model. For earthquakes where a preferred co-seismic slip distribution model is available, a web repository of the slip distribution files has been created at info.geonet.org.nz/x/TQAdAQ. All of the rupture models are provided in a common file format. Although the Inangahua and Edgecumbe earthquakes also have slip models determined from geodetic data [36, 38], these are not well constrained by data and hence are not provided on the web repository.

Fifteen earthquakes have fault dimensions that have been approximated from aftershock distributions. These approximate dimensions have been extracted from special studies, which are indicated in the references in Table 1.

To summarise, a total of 30 earthquakes in the New Zealand Strong Motion Database have either a published slip model, or published fault geometry. Table 1 shows the following variables from these events: strike angle; dip angle; rake angle; depth to the top of rupture (Z_{TOR}); fault length (L); fault width (W); the top centre latitude; and, the top centre longitude. However, due to the multi-segment ruptures of the Edgecumbe and Darfield earthquakes, no length, width, or top centre co-ordinates are given for these events, and the strike, dip and rake angle correspond only to the dominant fault segment. For the complex rupture of the 13 June 2011 Christchurch earthquake [60], no fault dimensions are given. The full source models for these events can instead be found at the web repository.

Inferred Fault Geometries

In addition to the 30 earthquakes with 'known' fault plane orientations and dimensions, we have indicated a preferred fault orientation for 57 other events. These preferred orientations are mostly for earthquakes that were deemed to have occurred on a subduction interface, as well as events where a given fault plane orientation is preferred based on regional tectonics. For the remaining events, no preferred fault orientations are indicated.

For the events where the fault dimensions are unavailable, indicative fault geometries have also been provided. First-order estimates of fault dimensions are inferred from M_0 and an assumed value for the stress drop $\Delta\sigma$, using the relation of Eshelby (1957) [66], for the case of a circular crack in a homogeneous, elastic, Poissondium with uniform stress drop:

$$r = \left[\frac{7}{16} \frac{M_0}{\Delta\sigma} \right]^{\frac{1}{3}} \quad (2)$$

where r is the source radius. M_0 values are available for all events, but $\Delta\sigma$ values are difficult to determine and observational studies tend to exhibit very large variability. In this study, average $\Delta\sigma$ values for various tectonic settings have been used in equation (2). The stress drop for each earthquake may differ significantly from this value, hence the purpose of the following values are only to provide a first-order estimate of the source dimension. For crustal events, a value of 5 MPa has been adopted, which is an average value for events in Canterbury [67], the Edgecumbe earthquake [68] and aftershocks of the Arthur's Pass earthquake [69]. The same 5 MPa value is adopted for subduction slab events, based on the observations of Hikurangi slab events by Reyners et al. (2010) [37], although recent work using an different method shows that stress drops for events around the Hikurangi Margin may average around 10 MPa [70]. For subduction interface events, a value of 2 MPa has been adopted, which is an average value determined for global subduction interface earthquakes [71]. For all of the events with inferred fault geometries, the hypocentre is assumed to be located in the centre of the fault plane.

DISTANCE METRICS

In addition to focal depth (h), epicentral distance (R_{epi}) and hypocentral distance (R_{hyp}), the following finite-fault distance metrics are provided in this database:

- The rupture distance, R_{rup}, defined as the shortest Cartesian distance between the recording site and the modelled fault.
- The Joyner-Boore distance, R_{jb}, defined as the distance between the recording site and the surface projection of the ruptured area.
- A hanging wall variable, R_x, defined as the station distance perpendicular to the fault strike from the surface projection of the up-dip edge of the fault plane.
- A second hanging wall variable, R_y, defined as the station distance parallel to the fault strike from the midpoint of the surface projection of the up-dip edge of the fault plane.
- The depth to the top of the rupture, Z_{TOR}.

Schematic examples of R_x, R_y and Z_{TOR} are shown in Figure 8. This figure is adapted from Chiou and Youngs (2008) [72]. For the 12 earthquakes with an available co-seismic slip distribution, the rupture areas are trimmed such that the model only includes areas with more than 50 cm of slip. The finite-fault distance metrics are then calculated from the trimmed fault plane. This is the same procedure that was adopted for the NGA-West2 database [15], and its purpose is to acknowledge that patches with little slip are unlikely to radiate large quantities of energy. For the 1968 Inangahua and 1987 Edgecumbe earthquakes, finite fault distances are calculated relative to published single-segment geodetic source models [36, 38], although there is considerable uncertainty in these values. Dowrick and Sritharan [73] calculated R_{rup} for Inangahua earthquake records relative to the geodetic slip model, and while their exact values could not be reproduced in

this study, the R_{rup} values calculated in this study are mostly within 1-2 km.

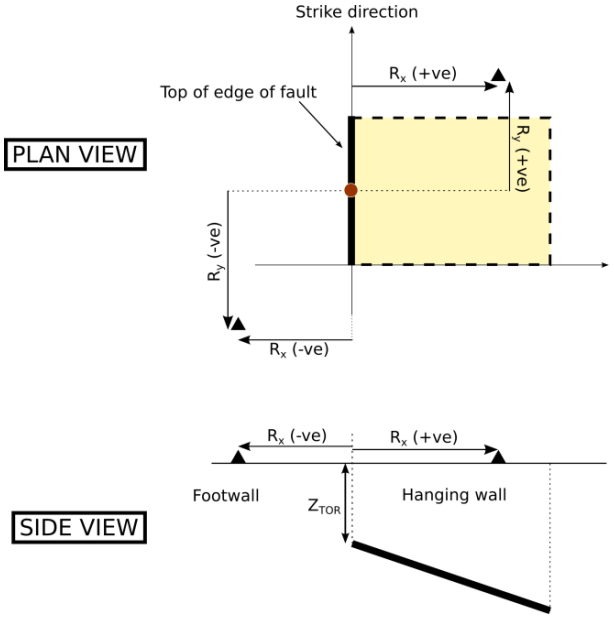

Figure 8: Schematic example showing calculation of variables R_x, R_y and Z_{TOR} (adapted from Chiou and Youngs, 2008).

For events where no preferred fault plane is available, the R_{rup} and R_{jb} values are taken as the average distances from the two orthogonal fault planes, determined using the circular crack models described earlier. However for these events, no R_x and R_y values are provided. For the earthquakes with ruptures consisting of multiple segments, R_x and R_y are calculated relative to closest segment. A comparison of the finite fault distances R_{rup} and R_{jb} to the hypocentral and epicentral distances respectively is shown in Figures 9a and 9b. Note that occasionally, R_{jb} is greater than R_{epi}. This is an illustration of the uncertainty in earthquake location, where the inverted slip distribution is in a different location to the preferred hypocentre. The $M_w - R_{rup}$ distribution of the records in the database is shown in Figure 10.

The final distance measure provided in the database is the volcanic path distance, R_{vol}, which is a variable that has traditionally been included in New Zealand ground motion models. To define the boundary for the Taupo Volcanic Zone (TVZ), the 'whole TVZ' model of Wilson *et al*. (1995) [74] was used, based on the recommendations of Cousins *et al.* (1999) [75]. Due to uncertainties in the depth extent for the whole TVZ model, this variable is only provided for events with focal depths less than 40 km, and is set to zero otherwise.

The provided distance measures are likely to be the most uncertain variables in the database. Absolute earthquake locations still tend to carry a lot of uncertainty, although the New Zealand velocity models, seismometer station spacings and the earthquake location methods are continually improving. It is difficult to provide meaningful statistical uncertainty measures for the distance variables, due to the problem of quantifying uncertainties in the velocity model. Hence no indications of distance uncertainty have been provided as part of this database. The distance uncertainties should be considered when analysing this database.

RECORD PROCESSING

In addition to calculating metadata related to the source and wave-propagation path, a database of uniformly-processed recordings has been developed. This is generally the most challenging task of database development, primarily due to the sheer volume of strong-motion accelerometric data currently available, and its highly variable quality. At the time of writing, the GeoNet strong-motion catalogue consists of nearly 70,000 recordings, beginning in 1966. In this study, strong motion recordings from this catalogue have been visually examined to remove low-quality recordings, and individually processed to remove any noise that is contaminating the signals. This analysis results in a database of 4,148 high-quality New Zealand strong-motion recordings.

The majority of the records have been collected since the introduction of GeoNet in 2001, as illustrated in Figure 11. While there were many significant events between 1968 and 2001, they tend to be poorly recorded due to the sparse network during this time period, and the lower quality of instruments. More than half of the data are recorded on the now-obsolete Etna instruments (Figure 12). The Basalt, EpiSensor and CUSP instruments collectively contribute around 35% of the recordings, and the remaining data are from older models operated prior to the introduction of GeoNet.

The processing of the records for the New Zealand Strong Motion Database differs from standard GeoNet processing [76]. The flowchart in Figure 13 summarises the differences between the two methods. Both methods take a 'Volume 1' recording as the input, which is the terminology for a digitised, uncorrected acceleration recording, and output a 'Volume 2', corrected recording. This terminology was introduced in the 1970s from Caltech data processing [77, 78]. While the Volume 1 records are usually referred to as 'uncorrected', in reality some processing has been applied to these records.

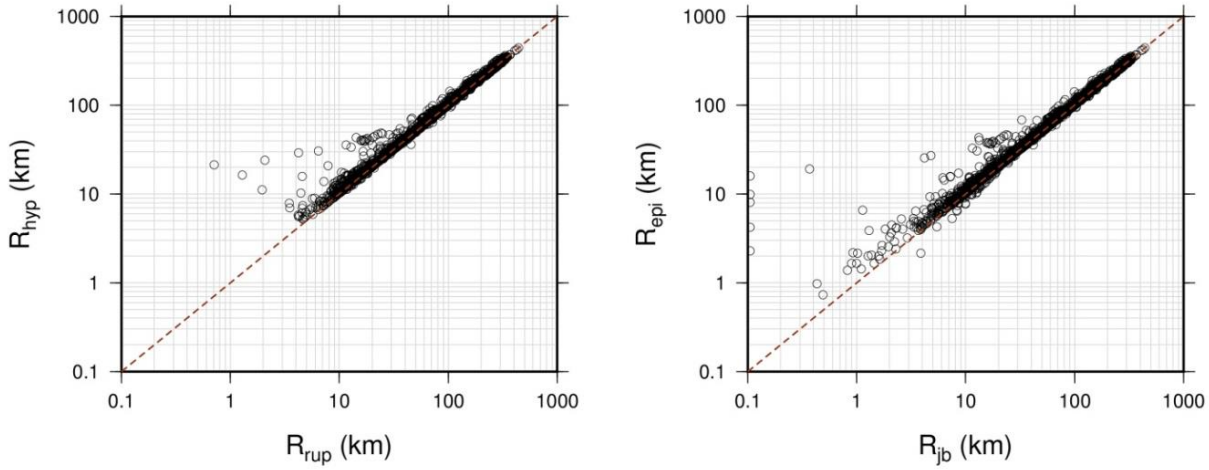

Figure 9: Comparison of finite fault distance metrics to point-source metrics, (left) rupture distance R_{rup} against hypocentral distance R_{hyp}, and (right) Joyner-Boore distance R_{jb} against epicentral distance R_{epi}. Values of R_{jb} = 0 km (representing stations situated directly on top of the rupture plane) are shown at 0.1 km, to enable plotting on a log scale.

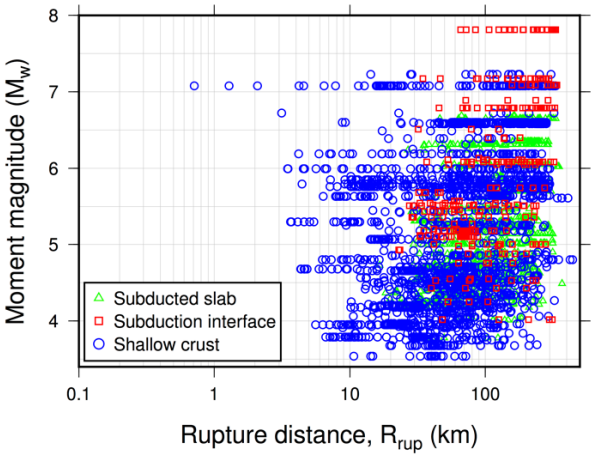

Figure 10: Magnitude-distance distribution of the recordings in the database.

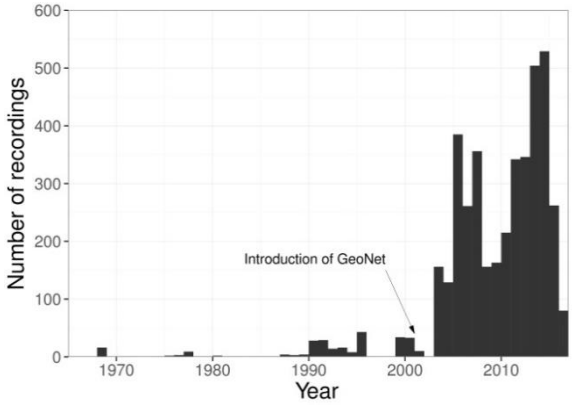

Figure 11: Number of high-quality strong-motion recordings in the New Zealand catalogue, against time.

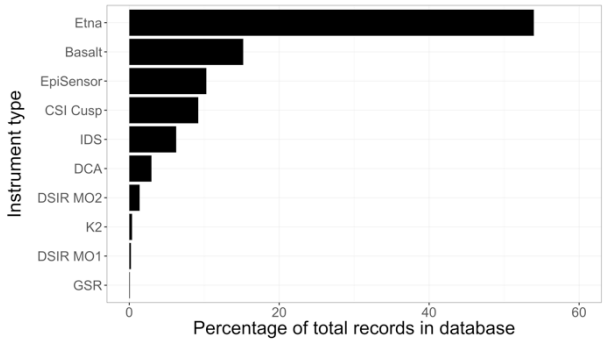

Figure 12: Proportion of recordings corresponding to each instrument type (excluding scratch plate data). Details of each instrument type can be found on the GeoNet website.

To obtain Volume 1 data, any baseline shifts in the raw accelerograms are removed and, where necessary, the data are converted to units of acceleration (mm/s^2) by removing the static sensitivity values. As part of the New Zealand Strong Motion Database project, the processing from raw accelerograms to Volume 1 files was not changed, but each step of the standard GeoNet Volume 1 to Volume 2 procedure was reviewed and tested. Findings of the reviews and descriptions of the changes from the standard GeoNet processing are detailed in the remainder of this section.

Removal of Mean

The first alteration to the standard GeoNet processing is with the mean-removal procedure, which currently removes the mean of the entire acceleration trace. This has now been changed to allow selection of pre-event windows, if available, from which the trace mean is removed. The reason for this alteration is to ensure the velocity and displacement traces start at approximately zero, and to retain the asymmetric character of some near-fault acceleration signals (e.g. one-sided velocity pulses).

Zero Padding

The standard GeoNet processing uses an acausal (zero-phase) filter to remove low-frequency noise, and the use of acausal filters result in long filter transients appearing in the time domain. The duration of the filter transient depends on the sharpness of the high-pass filter's frequency response. Before using acausal filters, acceleration signals must be zero-padded in the time domain to account for the filter transient, to ensure correct computation of velocity and displacement waveforms. For the standard GeoNet processing, Hodder (1983) [76] adds five seconds to the start and end of all processed time-series (i.e. a total of ten seconds). Converse & Brady (1992) [79] and Boore (2005) [80] suggest that the length of zero-padding should equal to:

$$T_{zpad} = \frac{1.5 nroll}{f_c} \tag{3}$$

where T_{zpad} is the zero-pad length in seconds, *nroll* is the filter roll-off parameter of a Butterworth filter (equal to half of the filter order) and f_c is the filter high-pass corner. Boore (2005) [80] also suggests that the zero pads should be retained in the processed Volume 2 files, for the distributed acceleration, velocity and displacement time-series to be compatible. For some strong-motion recordings, equation (3) leads to very long pre-event zero pads (e.g. *nroll* = 1, f_c = 0.02 Hz, and T_{zpad} = 75 seconds), which greatly increases the data storage requirements if all of the zero pads are to be retained. However, it was found that the GeoNet procedure, which retains a fixed ten seconds of the padded portion of the time-series, is sufficient for displacement time-series to be satisfactorily recovered from the partially pad-stripped accelerations, even when f_c = 0.02 Hz. Therefore, no modifications to this standard GeoNet processing step have been made for the New Zealand Strong Motion Database, and ten seconds of the padded time-series are included in the Volume 2 files.

High-Pass Filtering

For routine strong-motion data processing, GeoNet uses a sinusoidal transition filter, which requires the selection of a transition band for the frequency response function to decay from unity to zero. The frequency response of the high-pass filter is as follows:

$$Y(f) = \begin{cases} 0 & 0 \le f \le f_T \\ \sin^2\left(\frac{\pi}{2}\frac{f - f_T}{f_I - f_T}\right) & f_T \le f \le f_I \\ 1 & f \ge f_I \end{cases}, \tag{4}$$

where f_I and f_T are the filter initiation and termination frequencies respectively. All Volume 2 data distributed by GeoNet use a default transition band of 0.10-0.25 Hz for the high-pass filter, which is recommended by Hodder (1983) [76] as a trade-off between retaining useful information and minimising the impulse response of the filter. However, many large magnitude earthquakes in the New Zealand Strong Motion Database have significant low-frequency energy beneath this frequency band e.g. less than 0.10 Hz, which forces the high-pass filter to have a narrower transition band.

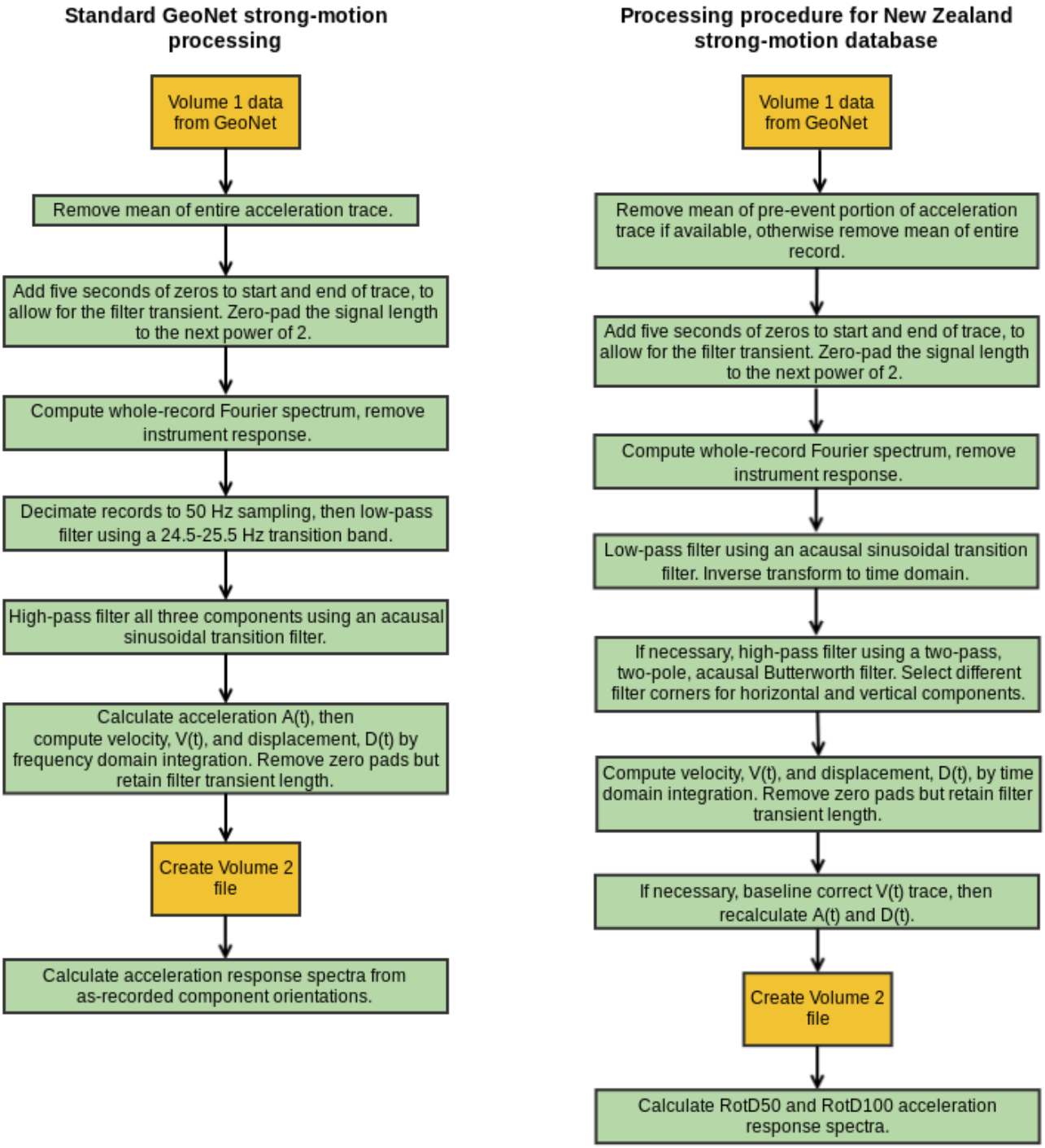

Figure 13: (Left) Summary of the standard GeoNet processing procedure (Hodder, 1983), and (right) summary of the New Zealand Strong Motion Database procedure.

Figure 14 shows the acceleration, velocity, and displacement impulse response of the sinusoidal transition filter for different transition bands, and compares this with the impulse response of a two-pole, two-pass Butterworth filter. While the sinusoidal transition filter performs well for the 0.10-0.25 Hz band, the duration of the displacement impulse response is much longer for the narrower transition band of 0.01-0.04 Hz. The two-pass, two-pole Butterworth filter has a slightly shorter impulse response than the sinusoidal transition filter. A further advantage of the Butterworth filter is that it is simple to control the shape of the filter, but the sinusoidal transition filter requires interpolation in log space if a preferred logarithmic fall-off rate is to be obtained. For these reasons, the Butterworth filter is adopted for high-pass filtering this collection of New Zealand strong motion data.

The frequency response of an acausal Butterworth filter is expressed by the following equation:

$$Y(f) = \frac{(f/f_c)^{2n}}{1+(f/f_c)^{2n}} \tag{5}$$

where n is the order of the filter. Figure 15 plots the frequency response of the Butterworth high-pass filter compared to the sinusoidal transition filter of Hodder (1983) [76].

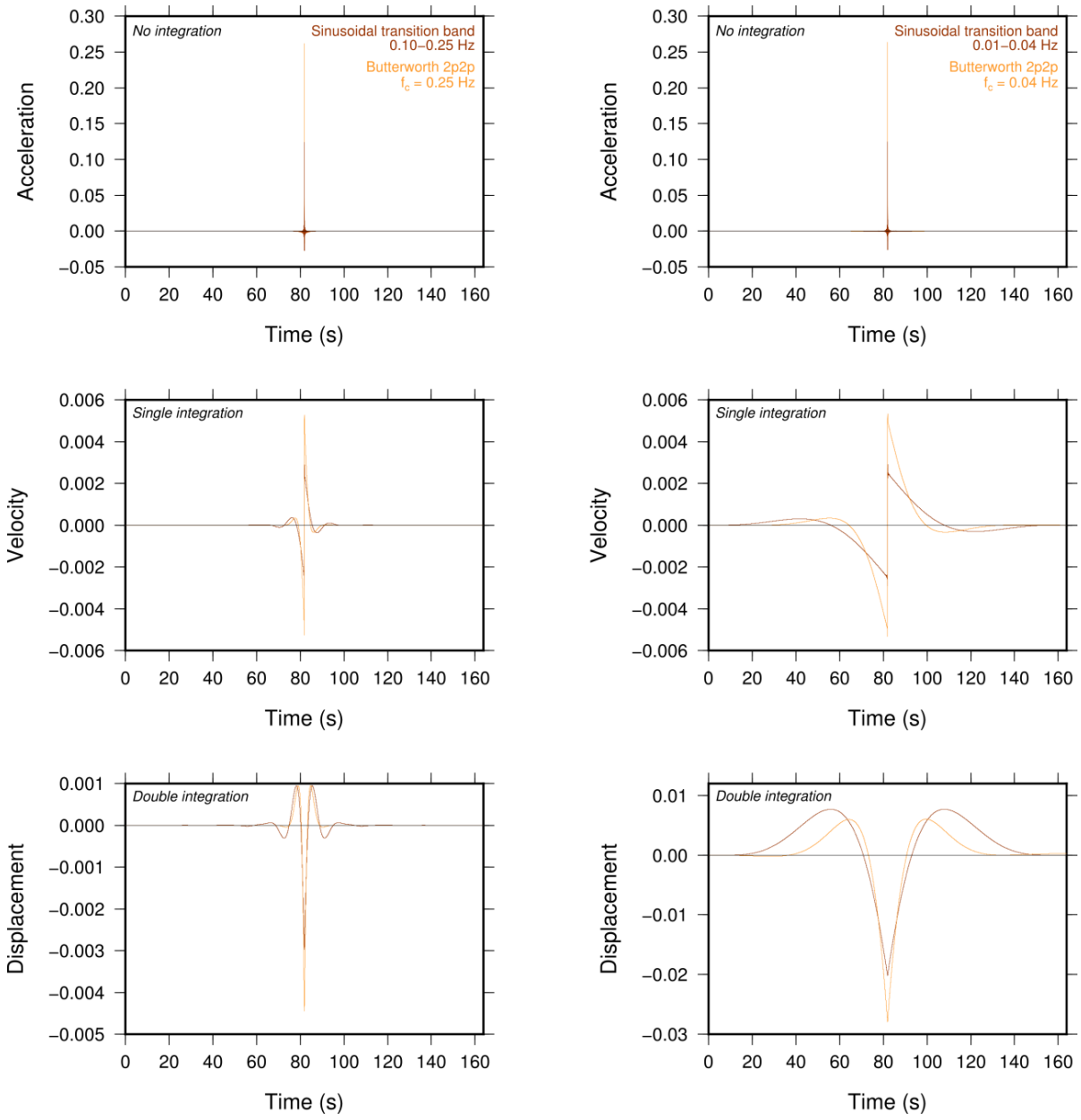

Figure 14: (Left) Comparison of the impulse response of a high-pass, sinusoidal filter with a 0.10-0.25 Hz transition band and a two-pass, two-pole, acausal, Butterworth high-pass filter with a corner frequency of 0.25 Hz. (Right) Same as left, but with a sinusoidal transition band of 0.01-0.04 Hz and Butterworth corner frequency of 0.04 Hz.

As noted by Ancheta *et al*. (2014) [15], an acausal Butterworth filter significantly reduces Fourier amplitudes at the filter corner (gain of -6 dB), and they suggest the minimum usable frequency for the data is where the frequency response of the filter is -1/2 dB. Adopting this criterion for the two-pass, two-pole acausal Butterworth high-pass filter used for the New Zealand database, the minimum usable frequency is 1.7 times the filter corner.

Separate filter corner frequencies are chosen for the vertical components of recordings in the database, but the same filter corner has been chosen for the two horizontal components, to ensure simple and robust calculation of average horizontal response spectra.

Decimation

Another feature of the standard GeoNet procedure is the decimation of recordings down to 50 Hz, then low-pass filtering in the 24.5-25.5 Hz transition band. The original purpose of the decimation was to reduce the data storage requirements, which was a problem at the time the procedure was developed but is less of an issue in the present day. In many cases, the removal of high-frequency information through decimation or low-pass filtering tends to have little influence on high-frequency pseudo-spectral acceleration values. This is because path and site attenuation usually removes the majority of high-frequency energy [81], and the amplitudes of high-frequency spectral accelerations are usually controlled by lower-frequency energy. However, Grazier (2012) [82] uses the GeoNet standard processing procedure to show that decimation and over-filtering of high-frequencies can result in the loss of critical information that affects high-frequency pseudo-spectral acceleration (PSA) values, and as a result the peak ground acceleration (PGA) can be erroneously reduced by up to 33%. In light of this work, recordings in the New Zealand Strong Motion Database are no longer decimated, and low-pass filter corners are selected on a record-by-record basis.

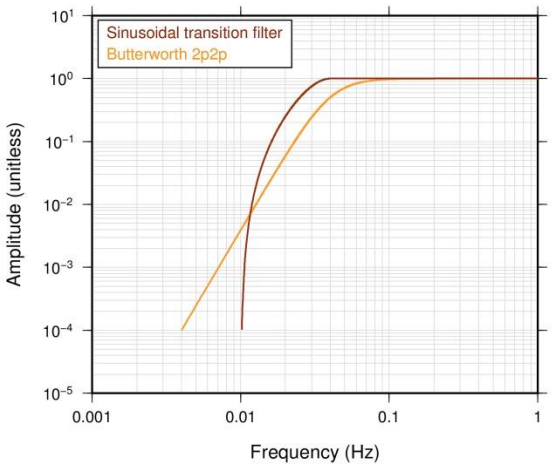

Figure 15: Frequency response of the two-pass, two-pole Butterworth high-pass filter with f_c = 0.04 Hz, and sinusoidal transition high-pass filters with a transition band between 0.01 and 0.04 Hz.

Low-Pass Filtering

The sinusoidal transition filter of Hodder (1983) [76] is preferred to a Butterworth filter for low-pass filtering. As the New Zealand strong motion waveform database has the dual purpose of providing both acceleration response spectra and Fourier amplitude spectra of acceleration, the objective is to remove high-frequency noise (to prevent adverse effects on high-frequency response spectral accelerations), while distorting the Fourier amplitudes as little as possible. The sinusoidal transition filter, with a transition bandwidth of 1 Hz, causes no observable ringing or rippling in the time and frequency domains of the signal respectively, and allows the usable bandwidth of the Fourier spectrum to extend up to the initiation frequency of the filter. The steeper decay of the sinusoidal transition filter, and the ease at which the maximum usable frequency can be defined, are attractive features of the sinusoidal filter that make it preferable to the Butterworth filter.

Baseline Correction

No baseline corrections are applied in the standard GeoNet processing procedure, with any distortions and offsets of the baseline being removed by the low-pass filtering. This method removes any evidence of permanent ground displacement in the signal, which arises from the fling-step effect. Boore (2001) [83] showed that it is difficult to find a baseline-correction procedure that can accurately recover the residual displacement, but found that acceleration and displacement response spectra are relatively insensitive to the type of baseline correction for oscillator frequencies less than 0.05 Hz. Figure 16 shows how the processing of signals with fling effects can affect the displacement time-history and acceleration response spectrum, for the DFHS recording from the 2010 Darfield earthquake. While the peak ground displacement (PGD) is a factor of three larger for the baseline-corrected recording than when the baseline offsets are removed by high-pass filtering, there is little influence on the acceleration response spectrum for frequencies greater than 0.04 Hz.

Burks & Baker (2014) [84] further investigated the effect of the signal processing of fling-step ground motions, and showed that the 'collapse capacity' of a nonlinear SDOF (single degree of freedom) system with a fundamental frequency of 0.33 Hz is not significantly affected by the signal processing (i.e. high-pass filtering or baseline correction). This indicates that the dynamic effects of fling may be preserved even if static offsets are removed by filtering. Despite these results, it is still unclear whether the static offsets will affect structures with lower fundamental frequencies than 0.33 Hz e.g. base-isolated structures. In order to provide the most realistic ground-motion time-series possible for future engineering purposes, efforts have been made to preserve static offsets in the New Zealand Strong Motion Database through baseline correction.

Unfortunately, a significant problem with baseline correction is subjectivity. Removing the baseline is effectively applying a high-pass filter to the data, and can be performed using a variety of different schemes, each of which represents a filter with different frequency response characteristics. As the cause of baseline offsets cannot be determined in many circumstances, there is no universally-accepted procedure for baseline correction. For the New Zealand Strong Motion Database, filtering is generally preferred over baseline-corrections, except where filtering results in loss of useful signal information, or leads to unrealistic response characteristics. For example, near-source recordings from the 2010 Darfield earthquake contain significant long-period energy down to 0.01 Hz. Rather than applying a high-pass filter with a corner frequency of 0.01 Hz, which results in large filter transients in the time-domain, the record-specific baseline-correction procedure described in Boore (2001) [83] was applied. While this scheme results in broadly similar permanent displacements to geodetic observations [85], the residual displacement of the baseline-corrected signal may not always be reliable, as the apparent static offsets may be caused by instrument errors or tilts, rather than by tectonic processes [86].

Comparison between New Zealand and PEER Processing

The procedure used to process the New Zealand database is slightly different from international processing routines. To compare the New Zealand database processing with that of the Pacific Earthquake Engineering Research (PEER) Center, response spectra from the 2010 Darfield and 2011 Christchurch earthquakes are examined. Recordings from these earthquakes were processed independently for the New Zealand Strong Motion Database and the NGA-West2 database [15], and therefore a direct comparison can be made between the two procedures. For 111 records from these two events, the ratios of response spectra calculated using the two routines are shown in Figure 17.

The response spectra calculated by the two different procedures are broadly similar. For 90% of the recordings, the differences in spectral accelerations are mostly within 10%. For a small number of recordings, significantly different choices of high-pass filter corners have resulted in large differences between the processing techniques at low oscillator frequencies. These recordings were identified and re-examined, but the original filter corners chosen for the New Zealand database were retained.

For other recordings, the New Zealand processing gives 15-20% higher spectral accelerations at oscillator frequencies around 10-20 Hz. The recordings with this discrepancy are all rock sites in the New Zealand National Seismograph Network with 50 Hz sampling rates. The PEER procedure uses a Butterworth filter for low-pass filtering, which has a more gradual roll-off than the sinusoidal-transition filter used for the New Zealand database. Rock-site recordings tend to have more high-frequency energy contributing to spectral accelerations at high oscillator frequencies. It is likely that the PEER filter is unintentionally removing some of this high-frequency energy, resulting in lower spectral accelerations. Overall, any differences in spectral accelerations as a result of the different processing procedures are considered minor.

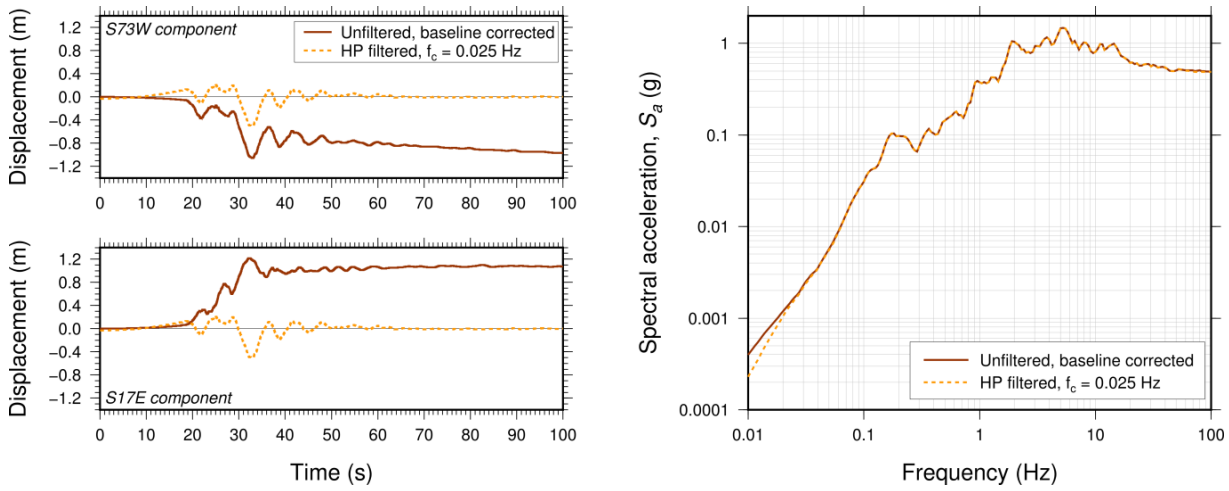

Figure 16: The effect of filtering and baseline correction on the displacement time-histories (left) from the DFHS recording from the 2010 Darfield earthquake, and (right) RotD50 acceleration response spectra. In this case, a simplified baseline correction procedure is used, by removing a straight line fit between the first and last points of the velocity trace.

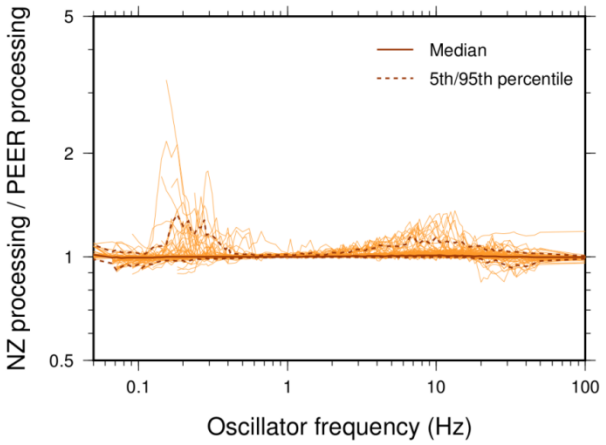

Figure 17: 5%-damped spectral acceleration ratio (New Zealand processing divided by the PEER NGA-West2 database processing) against oscillator frequency for 111 recordings from the Darfield and Christchurch earthquakes.

VISUAL REVIEWS OF RECORDINGS

Data Screening

For each three-component recording, the acceleration, velocity and displacement time-series and Fourier amplitude spectra of acceleration were visually examined for quality. Records were discarded if there were problems with the waveforms e.g. glitched signals or clipping. Excessively noisy signals were discarded such that the maximum permissible high-pass filter corner was 1 Hz and the minimum permissible low-pass filter initiation frequency was 10 Hz.

Records were also discarded if part of the signal was missing, such that the maximum motions were likely to have been missing. This occurs frequently for older events in the database, particularly where the recording instrument triggered on the S-wave arrival, rather than the P-wave arrival. For these records, the horizontal components were only retained if the largest signal amplitudes were likely to be captured by the remaining S-wave, coda and surface-wave portion of the signal. However, the vertical component was always removed for late-triggered recordings, as the largest signal amplitudes for vertical traces can occur in the vicinity of the P-wave arrival.

In addition, several near-source recordings from the Canterbury earthquake sequence were removed if they were from a site where surface liquefaction was observed (as indicated on the liquefaction maps of [87]), as liquefaction is not an effect that is typically considered in ground motion modelling. Those interested in examining these data can obtain the records from GeoNet's standard strong motion data repository (ftp.geonet.org.nz/strong/processed/Proc).

In some cases, the vertical trace was discarded due to poor quality, but the horizontal components could be retained. If one of the two horizontal components was deemed to be of poor quality, both horizontal components were discarded. This was to ensure that orientation-independent horizontal spectral accelerations could be calculated for all records in the database. This has resulted in a different number of horizontal response spectra than vertical response spectra in the database (4,148 vs 3,596 respectively).

Selection of High-Pass Filter Corners

To select the high-pass filter corner, first the Fourier amplitude spectra of acceleration (FAS) are plotted for all three components of the signal. To determine where the noise level exceeds the signal at low frequencies, a line that is consistent with increasing proportional to f^2 is plotted through the point corresponding to the maximum of the filtered displacement spectrum. If the low-frequency spectrum is increasing at a shallower rate than this line, it may be an indication that noise is contaminating the earthquake signal at these frequencies. This procedure [88] ensures that the peak spectral displacements of the processed record are not produced by long-period noise, which is indicated by a flat low-frequency portion in the unfiltered Fourier amplitude spectrum of acceleration (e.g. the portion of the spectrum in Figure 18 at frequencies lower than about 0.02 Hz). A low-frequency shape of the FAS of acceleration proportional to f^2 is also consistent with the Brune (1970) model of the far-field source spectrum, for frequencies lower than the corner frequency, f_c.

An example of the selection of a high-pass filter corner, f_{HP}, is shown in Figure 18. Using the chosen filter parameters, the final acceleration, velocity and displacement time-series were then reviewed for problems, such as long-period noise in the displacements, or if the velocities and displacements appear unphysical. Figure 19 compares the unfiltered and filtered acceleration, velocity and displacement time-series for the recording shown in Figure 18.

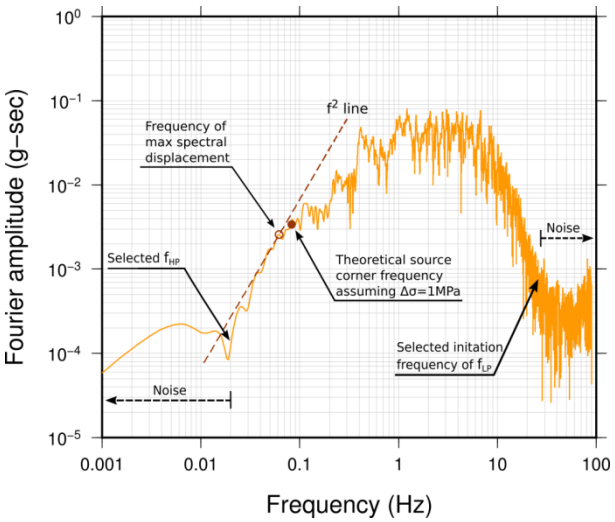

Figure 18: Example of high-pass and low-pass filter selection for the WDFS recording from the M_w6.6 Cook Strait earthquake in July 2013, showing the unfiltered Fourier amplitude spectrum of acceleration.

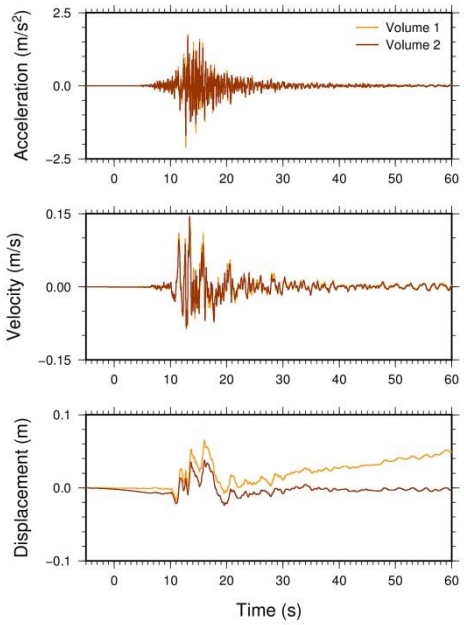

Figure 19: Comparison of unfiltered (Volume 1) and filtered (Volume 2) acceleration, velocity and displacement traces for the WDFS recording (S15E component) from the Mw6.6 Cook Strait earthquake in July 2013, using the filter parameters shown in Figure 18. Time starts at -5 s due to zero-padding of the Volume 1 waveforms.

For a large number of records in the database, the selected high-pass filter corner frequency may be higher than the source corner frequency. Figure 20 shows the chosen filter corners against magnitude, along with the Brune (1970) [89] source corner frequency assuming two alternative values for stress parameter $\Delta\sigma$ = 1 and 5 MPa. The latter value is the average stress parameter determined for the Canterbury earthquakes dataset by Oth and Kaiser (2014) [67]. While Akkar and Bommer (2006) [90] recommend discarding recordings with the high-pass filter frequency greater than the source corner frequency, this criterion is difficult to enforce given that the stress parameter is unknown for most events, and varies strongly between events. For this reason, the records have been retained in the database, however researchers using this database should consider how this issue will affect their analysis.

Selection of Low-Pass Filter Parameters

The selection of the low-pass filter parameters tends to be more straight-forward than the high-pass filter. High-frequency Fourier amplitudes of earthquake signals tend to decay exponentially because of path and site attenuation (modelled by Q and κ_0 respectively), hence it is generally very clear where the exponential decay of the signal amplitudes become flat when the signal decreases beneath the amplitudes of the noise level. The low-pass sinusoidal transition filter requires the selection of an initiation frequency, f_I, and a termination frequency, f_T. For the New Zealand database, the transition bandwidth was fixed at 1 Hz, following Hodder (1983) [76]. Figure 18 shows an example of how f_I is chosen.

Flagging Potentially Problematic Recordings

Recordings with known, strong, source effects, such as directivity or fling steps, have been identified and flagged. There are two reasons for this flag: 1) these records may need to be treated separately in ground-motion prediction equations; and 2) it allows records exhibiting velocity pulses to be easily identified for ground-motion selection in the time-domain analysis of structures. For recordings in the Canterbury earthquake sequence, this flag has already been calculated by Joshi (2013) [91], using the pulse identification algorithm of Shahi & Baker (2014) [92] in conjunction with manual interpretation of the results. However, for the remainder of the dataset, this has yet to be analysed and hence all other records are flagged as 'neutral directivity'. It is expected that a more complete representation of recordings in New Zealand that exhibit characteristic near-fault effects will become available in the future.

Records with a late trigger have also been flagged. These records have been interpreted to contain the maximum motions that occurred at the site (i.e. the horizontal response spectra are considered valid), but other researchers or practitioners may prefer to exclude these records from their analyses.

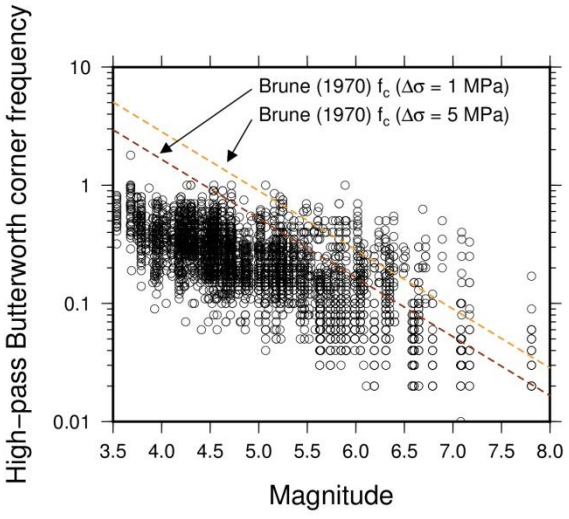

Figure 20: The high-pass Butterworth filter corner frequencies that have been selected for horizontal recordings in the database, compared with the theoretical Brune (1970) source corner frequency assuming stress parameters of 1 and 5 MPa.

CALCULATION OF RESPONSE SPECTRAL ORDINATES

Many previous ground motion models adopt the geometric mean spectral acceleration of two horizontal components to represent the average horizontal ground motion intensity, however this measure depends on the as-recorded sensor

orientations. The New Zealand Strong Motion Database instead provides orientation-independent RotDnn response spectra [93], where 'Rot' signifies that the horizontal time-series are rotated between 0 and 180˚, where for any rotation angle θ and as-recorded horizontal components $a_1(t)$ and $a_2(t)$,

$$a_{ROT}(t,\theta) = a_1(t)\cos(\theta) + a_2(t)\sin(\theta) \quad (6)$$

the 'nn' denotes the fractile of the spectra (i.e. nn = 50 is the median, and nn = 100 is the maximum) and the 'D' indicates that the rotations are specific to each oscillator period. The New Zealand Strong Motion Database provides RotD50 and RotD100 (i.e. average horizontal and maximum horizontal respectively) acceleration response spectra for 1, 2, 3, 5, 7, 10, 15, 20, 25, 30 and 40% oscillator damping. The response spectra have been calculated by evaluating Duhamel's integral at 22 frequencies between 0.1 and 100 Hz.

The minimum usable frequency of the response spectra is defined as 1.7 times the high-pass filter corner. The maximum usable frequency is more difficult to determine, as the low-pass filter of this study is much steeper than the likely high-frequency shape of the earthquake Fourier spectrum. While Douglas & Boore (2011) [81] find that accurate response spectra can be obtained up to 100 Hz regardless of the low-pass filtering, this largely depends on the characteristics of the recording. For example, a rock recording with a low rate of decay of the high frequencies may still have significant energy at frequencies above the low-pass filter frequency, and this can have a large effect on the high-frequency response spectral ordinates. Akkar *et al*. (2011) [94] opted to discard records where the filtered spectral acceleration differed by more than 10% from the unfiltered spectral acceleration, however this criterion is difficult to apply to many older recordings in the New Zealand database, which have a Nyquist frequency of 25 Hz. Rather than discarding potentially informative recordings, this study adopts the approach of Ancheta *et al*. (2014) [15], where it is assumed that the high-frequency filtering has a negligible effect on the high-frequency spectral accelerations and PGA, and the maximum usable frequency is 100 Hz. The left frame of Figure 21 plots the number of usable pseudo-spectral acceleration values against oscillator frequency.

Only RotD50 and RotD100 response spectra are provided in the database. For some applications, it may be of research interest to calculate the fault-normal and fault-parallel acceleration response spectra. However, large earthquakes often have complex geometries with ruptures on multiple faults (for example the 2010 Darfield and June 2011 Christchurch earthquakes [60]), and this complicates the definition of fault-normal and fault-parallel directions. For this reason, these spectra are not provided as part of this database, however interested researchers may calculate response spectra at any desired orientation from the processed time-series.

CALCULATION OF FOURIER SPECTRAL ORDINATES

Fourier amplitude spectra (FAS) of acceleration, calculated from the whole time-series using the Cooley-Tukey Fast Fourier Transform algorithm [95], are also supplied as part of the New Zealand Strong Motion Database. It is preferable for Fourier amplitudes to be calculated at the same frequency steps for all recordings, and to achieve this, a constant signal duration is necessary. The majority of records in the database have 50, 100 or 200 Hz sampling rates (time-steps of 0.02, 0.01 and 0.005 s respectively) for which it is simple obtain a common duration. These records are zero-padded to long durations, such that the number of data points for recordings sampled at 50, 100 and 200 Hz is 2^{16}, 2^{17} and 2^{18} respectively. In this case, the common duration is 1310.72 s. One station in the database, a Global Seismograph Network station in South Karori (GeoNet station code SNZO), samples at 80 Hz. For recordings from this station, the common duration is 204.8 s and 2^{14} samples. To downsample the calculated Fourier amplitude spectra to a more manageable number of data points, the FAS are smoothed to 100 equally-spaced points per decade on a log scale between 0.1 and 100 Hz, using a Konno & Ohmachi (1998) [96] filter with a b-value equal to 40.

Different variants of the average horizontal component are provided. For many applications, the 'geometric mean' horizontal FAS will be most appropriate. However, other analysts may prefer to use an orientation-independent averaging of the horizontal components. For this purpose, the quadratic mean spectrum of the two horizontal components is also provided, i.e.

$$Y_{qm}(f) = \sqrt{\frac{1}{2}\left(|Y_1(f)|^2 + |Y_2(f)|^2\right)} \quad (7)$$

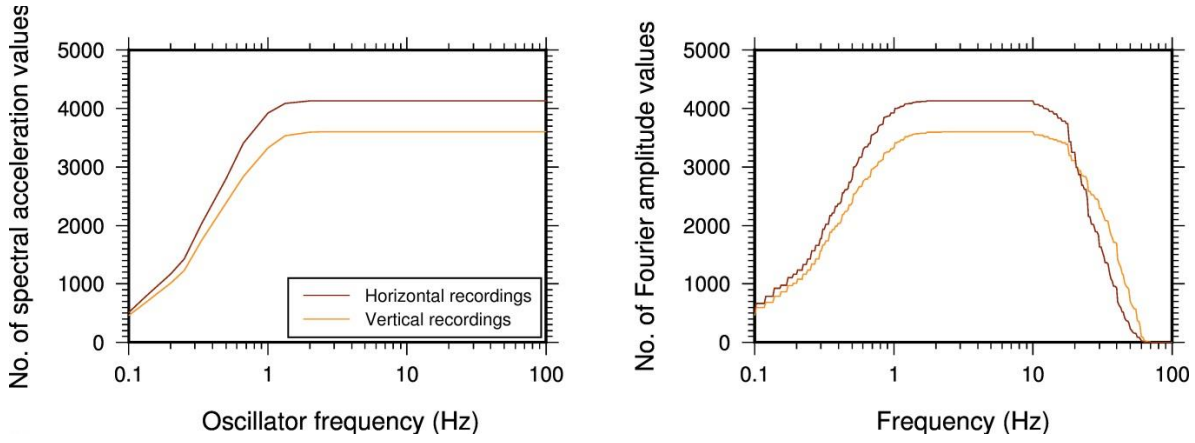

Figure 21: (Left) Total number of available horizontal (dark lines) and vertical (light lines) spectral acceleration values at each oscillator frequency, and (right) same as left, but for the number of usable Fourier amplitudes against frequency for horizontal and vertical spectra.

where $Y_1(f)$ and $Y_2(f)$ are the Fourier amplitude spectra of the two as-recorded horizontal components, and Y_{qm} is the quadratic mean spectrum. For these spectra, the smoothing is performed on the energy spectral density (square of the FAS). An example of smoothed and unsmoothed Fourier amplitude spectra for a recording in the New Zealand database is shown in Figure 22. The right frame of Figure 21 shows the number of usable Fourier amplitudes of acceleration against frequency.

Similar to the response spectral database, some researchers may be interested in analysing Fourier amplitude spectra at a given horizontal orientation, or may be interested in analysing the phase spectrum. As processed time-series are distributed as part of the New Zealand Strong Motion Database, Fourier spectra at any rotation angle can be calculated from the orthogonal horizontal time-series.

SCRATCH PLATE DATA

In addition to the response and Fourier spectra, scratch plate data are provided for the 1968 Inangahua and 1987 Edgecumbe earthquakes. As the original records could not be easily located, RotD50 values are not determined. Instead, only geometric mean and RotD100 PGA values are calculated, using the data given in Dowrick & Sritharan (1993) [73] and Cousins *et al*. (1988) [97].

ACCELEROGRAMS FOR STRUCTURAL ANALYSES

While there are 4,148 recordings in the strong-motion database, not all of these records are suitable for time-domain analysis of structures. A key consideration for the selection of accelerograms, which is often neglected in practice, is the high-pass filtering. For structures that are sensitive to low frequencies, it is important that the records also contain useful information at low frequencies. It is recommended that only records where the lowest usable frequency is less than or equal to 0.1 Hz (i.e. longest usable period greater than or equal to 10 s) should be used in time-domain structural analysis. Additionally, only records of sufficient duration to capture all significant body and surface wavetrains should be used. Should engineers wish to use New Zealand records for their structural analysis, the online webpage includes a list of 598 accelerograms in the database that are considered usable for structural analyses. All of these records, with the record-specific processing applied, are available from http://info.geonet.org.nz/x/TQAdAQ.

This is not considered a complete list of records that may be required for structural analysis, and for large magnitude (particularly scenarios representing Hikurangi subduction, Alpine Fault and Wellington Fault events, among others), accelerograms will need to be gathered from overseas catalogues.

CONCLUSION

This study has compiled strict and consistent source and path metadata from strong New Zealand earthquakes. This information is combined with waveform information and site metadata [1] into a publicly-available database. This database can be considered a source of high-quality New Zealand earthquake data, which can be used in seismic hazard and risk studies. In particular, it is anticipated that this database will have a key role in testing the applicability of overseas strong-motion seismology research to New Zealand tectonic environment (e.g. [98]).

The standard GeoNet strong-motion processing procedure has been modified for the New Zealand Strong Motion Database. While the GeoNet procedure performs well for most recordings in the database, the modifications have been made to ensure every recording is the best possible representation of the earthquake ground-motion. In particular, the updated processing provides more realistic waveforms for the large-magnitude, short-distance recordings that are of great engineering interest.

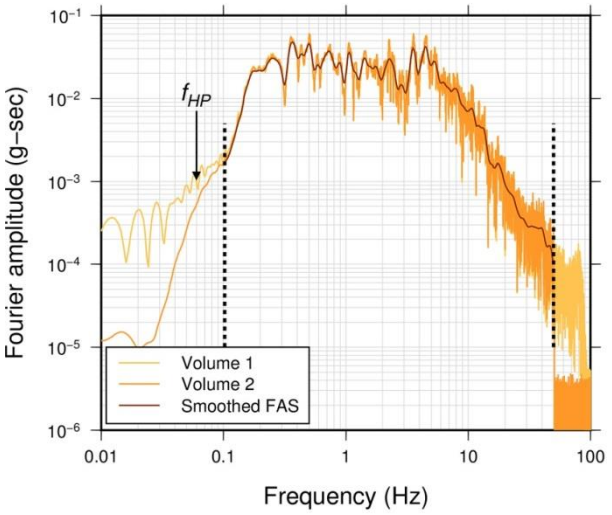

Figure 22: An example of a smoothed Fourier amplitude spectrum of acceleration for the CACS recording from the 13 June 2011 M6 Christchurch earthquake, compared to unsmoothed Volume 1 and Volume 2 Fourier spectra. 'f_{HP}' corresponds to the high-pass filter corner, and dashed vertical lines represent the usable frequency range of the Fourier spectrum (lower limit corresponding to 1.7 times the high-pass filter corner, upper limit corresponding to initiation frequency of low-pass filter).

There has been a strong focus on making the database useful for a number of different applications. In particular, a subset of the provided time-series provided may be used as input for time-domain analysis of structures, the horizontal and vertical response spectral data may be used for ground motion model development, ground-motion simulation validation or other engineering seismology research, and the Fourier spectra may be used in a variety of earthquake seismology studies. It is intended to keep this database reasonably up-to-date as large events continue to be recorded around the country. In the future, our intention is to further update the database with additional events and recordings as the relevant data become available, as well as adding new variables where possible.

ACKNOWLEDGMENTS

This article collates a vast amount of strong-motion seismology research that has occurred around New Zealand, and we greatly thank all of the researchers whose work has contributed to this database. While there have been many prolific contributors, Jim Cousins' efforts require special mention. Additionally, the guidance and oversight of Matt Gerstenberger greatly increased the database quality. Two GNS internal reviewers and Brendon Bradley are thanked for their comments on the manuscript. We also acknowledge the GeoNet project and its sponsors, the Earthquake Commission (EQC), GNS Science, and Land Information New Zealand (LINZ) for providing open access to the seismic data used in this study. Those behind the Canterbury accelerograph network (CanNet) [100] are acknowledged for their contribution towards the spatially-dense dataset from the Canterbury earthquake sequence. The study was funded by GNS Science Core Funding project number 410UET61-00, with contribution from National Hazards Research Platform (NHRP) project 'Rethinking PSHA'.

REFERENCES

1 Kaiser A, Van Houtte C, Perrin N, Wotherspoon L and McVerry G (2017). "Site characterisation of GeoNet stations for the New Zealand strong motion database". *Bulletin of the New Zealand Society for Earthquake Engineering*, **50**(1): 39-49.

2 Zhao J, Dowrick D and McVerry G (1997). "Attenuation of peak ground accelerations in New Zealand earthquakes". *Bulletin of the New Zealand National Society for Earthquake Engineering*, **30**(2): 133-158.

3 Stafford P (2006). "*Engineering seismological studies and seismic design criteria for the Buller region, South Island, New Zealand*". (PhD Thesis), University of Canterbury, Christchurch, New Zealand, 342 p.

4 Zhao J and Gerstenberger M (2010). "*Ground-motion prediction models for post-earthquake rapid reporting and reliable loss modelling using a sparsely distributed recording network in New Zealand*". GNS Science Consultancy Report, 2010/123, GNS Science, Lower Hutt, New Zealand, 82 p.

5 Kanamori H (1977). "The energy release in great earthquakes". *Journal of Geophysical Research*, **82**(20): 2981-2987.

6 Kagan Y (2002). "Modern California earthquake catalogs and their comparison". *Seismological Research Letters*, **73**(6): 921-929.

7 Anderson H, Webb T and Jackson J (1993). "Focal mechanisms of large earthquakes in the South Island of New Zealand: implications for the accommodation of Pacific-Australia plate motion". *Geophysical Journal International*, **115**(3): 1032-1054.

8 Webb T and Anderson H (1998). "Focal mechanisms of large earthquakes in the North Island of New Zealand: slip partitioning at an oblique active margin". *Geophysical Journal International*, **134**(1): 40-86.

9 Dziewonski A, Chou TA and Woodhouse J (1981). "Determination of earthquake source parameters from waveform data for studies of global and regional seismicity". *Journal of Geophysical Research: Solid Earth (1978–2012)*, **86**(B4): 2825-2852.

10 Matcham I, Savage M, Taber J and Reyners M (2006). "Earthquake source mechanism analysis for events between 1992 and 1997 using sparse New Zealand broadband data". *New Zealand Journal of Geology and Geophysics*, **49**(1): 75-89.

11 Ristau J (2008). "Implementation of routine regional moment tensor analysis in New Zealand". *Seismological Research Letters*, **79**(3): 400-415.

12 Ristau J (2013). "Update of regional moment tensor analysis for earthquakes in New Zealand and adjacent offshore regions". *Bulletin of the Seismological Society of America*, **103**(4): 2520-2533.

13 Dowrick D and Rhoades D (1998). "Magnitudes of New Zealand earthquakes, 1901-1993". *Bulletin of the New Zealand National Society for Earthquake Engineering*, **31**(4): 260-280.

14 Ristau J (2009). "Comparison of magnitude estimates for New Zealand earthquakes: moment magnitude, local magnitude, and teleseismic body-wave magnitude". *Bulletin of the Seismological Society of America*, **99**(3): 1841-1852.

15 Ancheta T, Darragh R, Stewart J, Seyhan E, Silva W, Chiou B, Wooddell K, Graves R, Kottke A, Boore D, Kishida T and Donahue J (2014). "NGA-West2 database". *Earthquake Spectra*, **30**(3): 989-1005.

16 Rhoades D (1997). "Estimation of attenuation relations for strong-motion data allowing for individual earthquake magnitude uncertainties". *Bulletin of the Seismological Society of America*, **87**(6): 1674-1678.

17 Stafford P (2014). "Crossed and nested mixed-effects approaches for enhanced model development and removal of the ergodic assumption in empirical ground-motion models". *Bulletin of the Seismological Society of America*, **104**(2): 702-719.

18 Zhao JX, Zhou S, Gao P, Long T, Zhang Y, Thio HK, Lu M and Rhoades D (2015). "An earthquake classification scheme adapted for Japan determined by the goodness of fit for ground-motion prediction equations". *Bulletin of the Seismological Society of America*, **105**(5): 2750-2763.

19 GeoNet (2015). *Earthquake Catalogue.* http://info.geonet.org.nz/display/appdata/Earthquake+Catalogue. Lower Hutt, New Zealand. (Accessed June 2015).

20 Reyners M, Eberhart-Phillips D and Bannister S (2011). "Tracking repeated subduction of the Hikurangi Plateau beneath New Zealand". *Earth and Planetary Science Letters*, **311**(1): 165-171.

21 International Seismological Centre (2013). *Online Bulletin.* http://www.isc.ac.uk/. International Seismological Centre, Thatcham, United Kingdom. (Accessed June 2015).

22 Lomax A, Virieux J, Volant P and Berge-Thierry C (2000). "*Probabilistic earthquake location in 3D and layered models*". Chapter 5 in *Advances in Seismic Event Location*, Springer, 101-134 p.

23 Lomax A, Michelini A and Curtis A (2009). "Earthquake location, direct, global-search methods". *Encyclopedia of Complexity and Systems Science*, Springer, New York. 2449-2473 p.

24 Smith W (1979). "*Documentation for earthquake location programs LOCAL and MICRO, and supporting software*". Technical Note: Geophysics Division, Department of Scientific and Industrial Research, Wellington, 35 p.

25 Bratt S and Nagy W (1991). "*The LocSAT program"*. Science Applications International Corporation, San Diego.

26 Kennett B (1991). "IASPEI 1991 Seismological Tables", *Terra Nova*, **3**(2): 122.

27 Eberhart-Phillips D, Reyners M, Bannister S, Chadwick M and Ellis S (2010). "Establishing a versatile 3-D seismic velocity model for New Zealand". *Seismological Research Letters*, **81**(6): 992-1000.

28 GeoNet (2015). *Origin Time, Location and Magnitude - Applications and Data - GeoNet.* http://info.geonet.org.nz/display/appdata/Origin+Time%2C+Location+and+Magnitude. (Accessed 16 December 2015).

29 Thurber C and Eberhart-Phillips D (1999). "Local earthquake tomography with flexible gridding". *Computers & Geosciences*, **25**(7): 809-818.

30 Thurber CH (1983). "Earthquake locations and three-dimensional crustal structure in the Coyote Lake area, central California". *Journal of Geophysical Research*, **88**(B10): 8226-8236.

31 Kennett B, Engdahl E and Buland R (1995). "Constraints on seismic velocities in the Earth from traveltimes". *Geophysical Journal International*, **122**(1): 108-124.

32 Bondár I and Storchak D (2011). "Improved location procedures at the International Seismological Centre". *Geophysical Journal International*, **186**(3): 1220-1244.

33 Williams C, Eberhart-Phillips D, Bannister S, Barker DH, Henrys S, Reyners M and Sutherland R (2013). "Revised interface geometry for the Hikurangi subduction zone, New Zealand". *Seismological Research Letters*, **84**(6): 1066-1073.

34 Eberhart-Phillips D and Reyners M (2001). "A complex, young subduction zone imaged by three-dimensional seismic velocity, Fiordland, New Zealand". *Geophysical Journal International*, **146**(3): 731-746.

35 Reyners M, Robinson R, Pancha A and McGinty P (2002). "Stresses and strains in a twisted subduction zone—Fiordland, New Zealand". *Geophysical Journal International*, **148**(3): 637-648.

36 Anderson H, Beanland S, Buck G, Darby D, Downes G, Haines J, Jackson J, Robinson R and Webb T (1994). "The 1968 May 23 Inangahua, New Zealand, earthquake: an integrated geological, geodetic, and seismological source model". *New Zealand Journal of Geology and Geophysics*, **37**(1): 59-86.

37 Reyners M, Eberhart-Phillips D and Ristau J (2010). "*Quantifying the hazard from New Zealand's shallow intraslab earthquakes*". Final report on EQC Project BIE, 08/549, GNS Science, Lower Hutt, New Zealand, 16 p.

38 Beanland S, Blick G and Darby D (1990). "Normal faulting in a back arc basin: geological and geodetic characteristics of the 1987 Edgecumbe earthquake, New Zealand". *Journal of Geophysical Research: Solid Earth (1978–2012)*, **95**(B4): 4693-4707.

39 Robinson R, Webb T, McGinty P, Cousins J and Eberhart-Phillips D (2003). "The 2000 Thompson Sound earthquake, New Zealand". *New Zealand Journal of Geology and Geophysics*, **46**(3): 331-341.

40 Reyners M, Gledhill K and Waters D (1991). "Tearing of the subducted Australian plate during the Te Anau, New Zealand, earthquake of 1988 June 3". *Geophysical Journal International*, **104**(1): 105-115.

41 McGinty P and Robinson R (1999). "Slip distribution of the Lake Tennyson earthquake, New Zealand, as inferred from static stress changes and off fault aftershocks". *Geophysical Research Letters*, **26**(13): 1961-1964.

42 Robinson R (1994). "Shallow subduction tectonics and fault interaction: the Weber, New Zealand, earthquake sequence of 1990–1992". *Journal of Geophysical Research: Solid Earth (1978–2012)*, **99**(B5): 9663-9679.

43 Luo X (1992). "Subduction interface and crustal structure in the Cape Palliser region, North Island, New Zealand, from observations of Cape Palliser earthquakes". *New Zealand Journal of Geology and Geophysics*, **35**(4): 491-499.

44 Abercrombie R, Webb T, Robinson R, McGinty P, Mori J and Beavan J (2000). "The enigma of the Arthur's Pass, New Zealand, earthquake: 1. Reconciling a variety of data for an unusual earthquake sequence". *Journal of Geophysical Research: Solid Earth (1978–2012)*, **105**(B7): 16119-16137.

45 Robinson R, Reyners M, Webb T, Arnadottir T, Beavan J, Cousins J, Van Dissen R and Pearson C (1995). "The Mw 6.7 Arthur's Pass earthquake in the Southern Alps, New Zealand, June 18, 1994". *Seismological Research Letters*, **66**(2): 11-13.

46 Gledhill K, Robinson R, Webb T, Abercrombie R, Beavan J, Cousins J and Eberhart-Phillips D (2000). "The Mw 6.2 Cass, New Zealand, earthquake of 24 November 1995: Reverse faulting in a strike-slip region". *New Zealand Journal of Geology and Geophysics*, **43**(2): 255-269.

47 McGinty P and Robinson R (2007). "The 2003 Mw 7.2 Fiordland subduction earthquake, New Zealand: aftershock distribution, main shock fault plane and static stress changes on the overlying Alpine Fault". *Geophysical Journal International*, **169**(2): 579-592.

48 Reyners M, McGinty P, Cox S, Turnbull I, O Neill T, Gledhill K, Hancox G, Beavan J, Matheson D and McVerry G (2003). "The Mw 7.2 Fiordland Earthquake of August 21, 2003: Background and Preliminary Results". *Bulletin of the New Zealand Society for Earthquake Engineering*, **36**(4): 233-248.

49 Petersen T, Ristau J, Beavan J, Denys P, Denham M, Field B, François-Holden C, McCaffrey R, Palmer N and Reyners M (2009). "The Mw 6.7 George Sound Earthquake of October 15, 2007: Responses and Preliminary Results". *Bulletin of the New Zealand Society for Earthquake Engineering*, **42**(2): 129-141.

50 François-Holden C, Bannister S, Beavan J, Cousins J, Field B, McCaffrey R, McVerry G, Reyners M, Ristau J and Samsonov S (2008). "The Mw 6.6 Gisborne earthquake of 2007: Preliminary records and general source characterisation". *Bulletin of the New Zealand Society for Earthquake Engineering*, **41**(4): 266-277.

51 Fry B, Bannister S, Beavan J, Bland L, Bradley B, Cox S, Cousins J, Gale N, Hancox G and Holden C (2010). "The Mw 7.6 Dusky Sound earthquake of 2009: Preliminary report". *Bulletin of the New Zealand Society for Earthquake Engineering*, **43**(1): 24-40.

52 Beavan J, Samsonov S, Denys P, Sutherland R, Palmer N and Denham M (2010). "Oblique slip on the Puysegur subduction interface in the 2009 July Mw 7.8 Dusky Sound earthquake from GPS and InSAR observations: implications for the tectonics of southwestern New Zealand". *Geophysical Journal International*, **183**(3): 1265-1286.

53 Beavan J, Motagh M, Fielding E, Donnelly N and Collett D (2012). "Fault slip models of the 2010–2011 Canterbury, New Zealand, earthquakes from geodetic data and observations of postseismic ground deformation". *New Zealand Journal of Geology and Geophysics*, **55**(3): 207-221.

54 Holden C, Beavan J, Fry B, Reyners M, Ristau J, Van Dissen R, Villamor P and Quigley M (2011). "Preliminary source model of the Mw 7.1 Darfield earthquake from geological, geodetic and seismic data". *In Proceedings of Proceedings of the Ninth Pacific Conference on Earthquake Engineering, Building an Earthquake-Resilient Society*, Auckland, New Zealand, 14-16 April, Paper No. 164.

55 Barnhart W, Willis M, Lohman R and Melkonian A (2011). "InSAR and optical constraints on fault slip during the 2010-2011 New Zealand earthquake sequence". *Seismological Research Letters*, **82**(6): 815-823.

56 Elliott J, Nissen E, England P, Jackson J, Lamb S, Li Z, Oehlers M and Parsons B (2012). "Slip in the 2010–2011 Canterbury earthquakes, New Zealand". *Journal of Geophysical Research: Solid Earth (1978–2012)*, **117**(B3).

57 Atzori S, Tolomei C, Antonioli A, Merryman Boncori J, Bannister S, Trasatti E, Pasquali P and Salvi S (2012). "The 2010–2011 Canterbury, New Zealand, seismic sequence: multiple source analysis from InSAR data and modeling". *Journal of Geophysical Research: Solid Earth (1978–2012)*, **117**(B8).

58 Holden C (2011). "Kinematic source model of the 22 February 2011 Mw 6.2 Christchurch earthquake using strong motion data". *Seismological Research Letters*, **82**(6): 783-788.

59 Serra EMT, Delouis B, Emolo A and Zollo A (2013). "Combining strong-motion, InSAR and GPS data to refine the fault geometry and source kinematics of the 2011, Mw

6.2, Christchurch earthquake (New Zealand)". *Geophysical Journal International*, **194**(3): 1760-1777.

60 Holden C and Beavan J (2012). "Source studies of the ongoing (2010-2011) sequence of recent large earthquakes in Canterbury". *In Proceedings of The 15th World Conference on Earthquake Engineering*, Lisbon, Portugal, 24-28 September.

61 Ristau J, Holden C, Kaiser A, Williams C, Bannister S and Fry B (2013). "The Pegasus Bay aftershock sequence of the Mw 7.1 Darfield (Canterbury), New Zealand earthquake". *Geophysical Journal International*, **195**(1): 444-459.

62 Holden C, Kaiser A, Van Dissen R and Jury R (2013). "Sources, ground motion and structural response characteristics in Wellington of the 2013 Cook Strait earthquakes". *Bulletin of the New Zealand Society for Earthquake Engineering*, **46**(4): 188-195.

63 Hamling I, D'Anastasio E, Wallace L, Ellis S, Motagh M, Samsonov S, Palmer N and Hreinsdóttir S (2014). "Crustal deformation and stress transfer during a propagating earthquake sequence: The 2013 Cook Strait sequence, central New Zealand". *Journal of Geophysical Research: Solid Earth*, **119**(7): 6080-6092.

64 Kaneko Y, Hamling I, Van Dissen R, Motagh M and Samsonov S (2016). "InSAR imaging of displacement on flexural-slip faults triggered by the 2013 Mw 6.6 Lake Grassmere earthquake, central New Zealand". *Geophysical Research Letters*, **42**(3): 781-788.

65 Kaiser A, Holden C, Hamling I, Hreinsdóttir S, Horspool N, Massey C, Villamor P, Rhoades D, Fry B, D'Anastasio E, Benites R, Christophersen A, Ristau J, Ries W, Goded T, Archibald G, Little C, Bannister S, Ma Q, Denys P, Pearson C, Giona-Bucci M, Almond P, Van Ballegooy S and Wallace S (2016). "The 2016 Valentine's Day Mw5.7 Christchurch earthquake: preliminary report". *In Proceedings of Conference of the New Zealand Society for Earthquake Engineering*, Christchurch, New Zealand, 1-3 April 2016, Paper number O-20.

66 Quigley M, Van Dissen R, Villamor P, Litchfield N, Barrell D, Furlong K, Stahl T, Duffy B, Bilderback E, Noble D, Townsend D, Begg J, Jongens R, Ries W, Claridge J, Klahn A, Mackenzie H, Smith A, Hornblow S, Nicol R, Cox S, Langridge R and Pedley K (2010). "Surface rupture of the Greendale fault during the Darfield (Canterbury) earthquake, New Zealand: initial findings". *Bulletin of the New Zealand Society for Earthquake Engineering*, **43**(4): 236-242.

67 Eshelby J (1957). "The determination of the elastic field of an ellipsoidal inclusion, and related problems". *Proceedings of the Royal Society of London A: Mathematical, Physical and Engineering Sciences*, **241**(1226): 376-396.

68 Oth A and Kaiser A (2014). "Stress Release and Source Scaling of the 2010–2011 Canterbury, New Zealand Earthquake Sequence from Spectral Inversion of Ground Motion Data". *Pure and Applied Geophysics*, **171**(10): 2767-2782.

69 Priestley K (1989). "Source parameters of the 1987 Edgecumbe earthquake, New Zealand". *New Zealand Journal of Geology and Geophysics*, **32**(1): 53-59.

70 Abercrombie R, Bannister S, Pancha A, Webb T and Mori J (2001). "Determination of fault planes in a complex aftershock sequence using two-dimensional slip inversion". *Geophysical Journal International*, **146**(1): 134-142.

71 Abercrombie R, Bannister S, Ristau J and Doser D (2016). "Variability of earthquake stress drop in a subduction setting, the Hikurangi Margin, New Zealand". *Geophysical Journal International*, **208**: 306-320.

72 Denolle M and Shearer P (2016). "New perspectives on self-similarity for shallow thurst earthquakes". *Journal of Geophysical Research: Solid Earth*, **121**: 6533-6565. doi: 10.1002/2016JB013105.

73 Chiou B and Youngs R (2008). "*NGA model for average horizontal component of peak ground motion and response spectra*", PEER Report 2008/09, Pacific Earthquake Engineering Research Center, Berkeley, United States, 293 p.

74 Dowrick D and Sritharan S (1993). "Peak ground accelerations recorded in the 1968 Inangahua Earthquake and some attenuation implications". *Bulletin of the New Zealand National Society for Earthquake Engineering*, **263**: 349-355.

75 Wilson C, Houghton B, McWilliams M, Lanphere M, Weaver S and Briggs R (1995). "Volcanic and structural evolution of Taupo Volcanic Zone, New Zealand: a review". *Journal of Volcanology and Geothermal Research*, **68**(1): 1-28.

76 Cousins W, Zhao J and Perrin N (1999). "A model for the attenuation of peak ground acceleration in New Zealand earthquakes based on seismograph and accelerograph data". *Bulletin of the New Zealand National Society for Earthquake Engineering*, **32**(4): 193-220.

77 Hodder S (1983). "Computer processing of New Zealand strong-motion accelerograms". *Bulletin of the New Zealand National Society for Earthquake Engineering*, **16**(3): 234-246.

78 Trifunac M (1971). "Zero baseline correction of strong-motion accelerograms". *Bulletin of the Seismological Society of America*, **61**(5): 1201-1211.

79 Trifunac M and Lee V (1978). "*Uniformly processed strong earthquake ground accelerations in the western United States of America for the period from 1933 to 1971: corrected acceleration, velocity and displacement curves*". Department of Civil Engineering, University of Southern California, Los Angelesp.

80 Converse A and Brady AG (1992). "*BAP: basic strong-motion accelerogram processing software, version 1.0*". United States Geological Survey Open-File Report, 92-296A, United States Geological Survey, Denver, Colorado, 174 p.

81 Boore D (2005). "On pads and filters: Processing strong-motion data". *Bulletin of the Seismological Society of America*, **95**(2): 745-750.

82 Douglas J and Boore D (2011). "High-frequency filtering of strong-motion records". *Bulletin of Earthquake Engineering*, **9**(2): 395-409.

83 Graizer V (2012). "Effect of low-pass filtering and re-sampling on spectral and peak ground acceleration in strong-motion recordings". *In Proceedings of 15th World Conference of Earthquake Engineering*, Lisbon, Portugal, 24-28 September,

84 Boore D (2001). "Effect of baseline corrections on displacements and response spectra for several recordings of the 1999 Chi-Chi, Taiwan, earthquake". *Bulletin of the Seismological Society of America*, **91**(5): 1199-1211.

85 Burks L and Baker J (2014). "Fling in near-fault ground motions and its effect on structural collapse capacity". *In Proceedings of Tenth US National Conference on*

Earthquake Engineering, Frontiers of Earthquake Engineering, Anchorage, Alaska, 21-25 July,

86 Beavan J, Wallace L, Samsonov S, Ellis S, Motagh M and Palmer N (2010). "The Darfield (Canterbury) earthquake: geodetic observations and preliminary source model". *Bulletin of the New Zealand Society for Earthquake Engineering*, **43**(4): 228-235.

87 Graizer V (2005). "Effect of tilt on strong motion data processing". *Soil Dynamics and Earthquake Engineering*, **25**(3): 197-204.

88 Canterbury Earthquake Recovery Authority (2012). *Geotechnical database for Canterbury Earthquake Sequence.* https://canterburygeotechnicaldatabase.projectorbit.com/. (Accessed 23/01/15).

89 Cousins WJ, Hefford R, McVerry G and Downer R (1987). "*Computer analyses of New Zealand earthquake accelerograms* ". 1981-1985, Physics and Engineering Laboratory, Department of Scientific and Industrial Research, Lower Hutt, New Zealand, 279 p.

90 Brune J (1970). "Tectonic stress and the spectra of seismic shear waves from earthquakes". *Journal of Geophysical Research*, **75**(26): 4997-5009.

91 Akkar S and Bommer J (2006). "Influence of long-period filter cut-off on elastic spectral displacements". *Earthquake Engineering and Structural Dynamics*, **35**(9): 1145-1165.

92 Joshi V (2013). "*Near-fault forward-directivity aspects of strong ground motions in the 2010-11 Canterbury earthquakes".* (Master of Engineering Thesis), University of Canterbury, Christchurch, New Zealand, 318 p.

93 Shahi S and Baker J (2014). "An Efficient Algorithm to Identify Strong-Velocity Pulses in Multicomponent Ground Motions". *Bulletin of the Seismological Society of America*, **104**(5): 2456-2466.

94 Boore D (2010). "Orientation-independent, nongeometric-mean measures of seismic intensity from two horizontal components of motion". *Bulletin of the Seismological Society of America*, **100**(4): 1830-1835.

95 Akkar S, Kale Ö, Yenier E and Bommer JJ (2011). "The high-frequency limit of usable response spectral ordinates from filtered analogue and digital strong-motion accelerograms". *Earthquake Engineering & Structural Dynamics*, **40**(12): 1387-1401.

96 Cooley JW and Tukey JW (1965). "An algorithm for the machine calculation of complex Fourier series". *Mathematics of Computation*, **19**(90): 297-301.

97 Konno K and Ohmachi T (1998). "Ground-motion characteristics estimated from spectral ratio between horizontal and vertical components of microtremor". *Bulletin of the Seismological Society of America*, **88**(1): 228-241.

98 Cousins WJ, Hefford R, McVerry G and O'Kane S (1988). "*Computer analyses of New Zealand earthquake accelerograms*". Ground records from the 1987 Edgecumbe earthquake, Physics and Engineering Laboratory, Department of Scientific and Industrial Research, Lower Hutt, New Zealand, 234 p.

99 Van Houtte C (2017). "Performance of response spectral models against New Zealand data". *Bulletin of the New Zealand Society for Earthquake Engineering*, **50**(1): 21-38.

100 Berrill J, Avery H, Dewe M, Chanerley A, Alexander N, Dyer C, Holden C and Fry B (2011). "The Canterbury Accelerograph Network (CanNet) and some results from the September 2010, M7.1 Darfield Earthquake.". *In Proceedings of The Ninth Pacific Conference on Earthquake Engineering, Building an Earthquake-Resilient Society*, Auckland, New Zealand, 14-16 April, 2011, Paper number 181.